The sedimentology, geomorphology, and hydrology of extreme floods on the Assiniboine River, southwestern Manitoba

by

Claire Morrow

A thesis submitted to the Faculty of Graduate Studies of

The University of Manitoba

in partial fulfillment of the requirements for the degree of

MASTER OF SCIENCE

Department of Earth Sciences
University of Manitoba
Winnipeg

ABSTRACT

River flooding is the most common natural disaster in Canada, particularly in the prairie provinces. Floods occur when river discharge exceeds the volume a channel is capable of conveying. Extreme floods on meandering rivers can cause significant geomorphic change, however, the extent to which the sedimentary record of extreme floods differs from that of annual floods is unclear. In the past decade, the Assiniboine River in southwestern Manitoba has experienced three >200-year-recurrence interval floods. Recent studies of local and global climatic changes have suggested a potential for more extreme precipitation events that lead to increased flood risk. The objectives of this thesis are to: i) investigate the sediments deposited by these extreme floods, and ii) quantify the drivers of flood hazard on the Assiniboine River. The goal is to refine our understanding of the sedimentary record of multiple extreme floods and evaluate the relative contributions of in-channel sedimentation and climatic factors to recent flooding events. This thesis combines qualitative field-based investigations of point-bar deposits with quantitative stream-gauge data analysis to achieve these goals.

Point bars in Spruce Woods Provincial Park have undergone extensive lateral migration over the past decade, with over 80% of migration occurring during three extreme flood events. The sedimentation associated with each flood event revealed that in some instances, extreme floods can generate an atypical coarsening upward profile of point-bar deposits. However, the deposits do not differ significantly from annual sedimentation, rather they are deposited more rapidly and in larger volumes. Data analysis of 60 years of stream-gauge data reveals that the greatest driver of flood hazard is an increase in flow frequency, however channel capacity changes have had a lesser but significant impact on decreasing the flood frequency. Climatic

changes, specifically intense rainfall events, are a potential driver of the increased flow frequency, but further work is required to evaluate anthropogenic factors that also contribute to overland flow (e.g., urbanization, monoculture farming, etc.). The results of this thesis contribute to the refinement of point-bar models, specifically the recognition criteria for extreme floods, and offer insight into the drivers of flood hazard on the Assiniboine River.

ACKNOWLEDGEMENTS

First and foremost, I would like to thank my advisor, Dr. Paul Durkin, for his endless guidance and support over the past three years. I greatly appreciate all the time and effort he has dedicated to my project. It would not have been the same without his contributions in the field and office. He has inspired and motivated me to be a better geologist and scientist, pushing me to always improve. He provided me endless opportunities for growth and education, never doubting me even when I doubted myself. I consider myself very fortunate to have had a supervisor such as Paul.

I must thank Trevin Ferens, Joel Kroeker, Katrina Mayo, and Levi Page for their incredible field assistance. It is no easy feat digging tens of trenches on a point bar and I could not have done it without you. I am thankful to my excellent committee members, Dr. Zou Zou Kuzyk and Dr. Jens Ehn, who were supportive and understanding through the unprecedented challenges of the past two and a half years. I appreciate Misuk Yun for their assistance with the lab work for this research, Meg Miller for guiding me through the trials and tribulations of ArcGIS, and Tyler Hodder of the MGS for his help with LiDAR data. I would also like to thank my fellow earth science graduate students for continually inspiring me as they pursued their research.

I am extremely grateful for my mom and dad, Sherry and Garry Morrow, and my stepmom, Lorraine Morrow, who have always allowed me to pursue my passions. I am the first person in my family to receive a bachelor's, and now a master's, and I could not have done it without their love, support, and encouragement. I am lucky to have found my "Manitoba Family" who gave me a home-away-from-home. Finally, to my partner, Julian, it was an absolute pleasure pursuing our master's degrees together.

TABLE OF CONTENTS

LIST OF TABLES

LIST OF FIGURES

CHAPTER ONE: INTRODUCTION

1.1. Motivation

The motivation for this thesis is a need to improve our understanding of the geomorphological impacts and sedimentological products of extreme floods, as well as the drivers of these high-discharge events. Meandering rivers are a significant landform, found in both modern environments and in the sedimentary record. They serve as political boundaries (e.g., Missouri River), economic thoroughfares (e.g., Mississippi River), and are significant groundwater aquifers and hydrocarbon reservoirs (e.g., Triassic St Bees Formation and Cretaceous McMurray Formation). As such, they have received considerable scientific interest, including numerous studies on the three-dimensional flow through meander bends (Bathurst et al., 1977; Dietrich, 1987; Blanckart, 2010) and sedimentological investigations that generated well-defined models of the resulting deposits (e.g., point bar fining upward profiles; Allen, 1965; McGowen & Garner, 1970; Bluck, 1971). The fining-upwards facies model can be directly related to the flow structure around the meander bend. At the bend entrance, flow is directed outwards from the bar towards the cutbank causing superelevation of the water surface. This causes a pressure gradient, driving flow along the bed of the channel towards and up the inner bank (Bathurst et al., 1977; Dietrich, 1987; Blanckaert, 2010). This results in coarser deposits along the bar head. As flow continues around the bend, it develops a secondary helical circulation downstream of the bend apex which, in addition to flow separation, deposits coarser sediments in the channel thalweg and finer sediments along the bar tail (Hooke, 1975; Leeder & Bridges, 1975). The study of point bar deposits is an exceptional example of integrating geomorphology with sedimentology to better understand the sedimentary record.

The geomorphology of meander bends and the sedimentology of point bars are intrinsically connected through the process of concurrent erosion and deposition. As water flows

through the meander bend it is eroding sediment from the cutbank and depositing sediment on the point bar, causing migration (Leopold & Wolman, 1960). River meander bends migrate laterally through expansion, translation, rotation, or a combination of the three (Daniel, 1971; Jackson, 1976). Expansion is the growth of a meander bend by an increase in path length, usually along the point-bar axis. Translation is the downstream migration of a point bar without a change in shape (Ghinassi et al., 2016). Rotation involves a change in the point bar axis as the bend changes orientation (Daniel, 1971). As this occurs, the morphology of the river and the surrounding river valley is altered.

Recently, significant progress has been made linking meander-bend morphodynamics to their resultant sedimentary deposits (Bridge et al., 1995; Burge & Smith, 1999; Smith et al., 2009). However, alongside this increased understanding of geomorphology and sedimentology comes the need to investigate new scientific questions that arise. It has become evident that the flow structure that is key to meander bends varies with flood stage, raising the question of whether deposits also vary at different flood stages (Kasvi et al., 2013; 2017; Ghinassi et al., 2018). Initial findings that modern meandering rivers produce variable deposits with variable discharge agree with formative studies that attribute a coarsening-upwards trend to extreme discharges (Costa, 1974; Fisk, 1974; Knox, 1987; Ghinassi et al., 2018). In this thesis, the goal is to evaluate whether extreme discharges have resulted in the formation of facies that deviate from the typical upward-fining facies model through field investigations of two point bars on the Assiniboine River in Spruce Woods Provincial Park, Manitoba, Canada. In the past decade, the Assiniboine River has experienced three high discharge events in 2011, 2014, and 2017. During these events, the two point bars of interest in this study underwent significant geomorphic change (i.e., Cut-offs; Fig 1.1). Due to extensive satellite imagery of the area and LiDAR

Fig 1.1. RPAS image of the Fallen Tree Point Bar (FTPB) with terrace edge and the 2010 abandoned channel highlighted.

collected following the 2014 extreme flood, we can correlate the results of point bar excavations to extreme flood deposits and typical flow deposits (Chapter 2).

The frequency and magnitude of these recent flooding events has raised the question of whether these events are related to climate change (Simonovic & Li, 2004; Rasmussen, 2015; Burn & Whitfield, 2016; Gauer et al., 2019). Flooding occurs when the discharge of a flow exceeds the capacity of the channel, breaching the river's banks and inundating the surrounding floodplain. An increase in flood hazard, therefore, may occur because of either an *increase* in frequency of extreme discharge or a *decrease* in capacity of the channel (i.e., the potential discharge a stream can convey). Traditionally, only discharge has been considered as a driver of flooding (Shrubsole et al., 2003; Co-operators, n.d.); however, recently bathymetric data has become increasingly integrated into flood hazard analysis. A study by Slater et al. (2015) on the capacity of rivers to convey flood discharges found that, in the United States, changes in flood hazard caused by channel capacity were smaller, but more common, than changes in flood hazard driven by discharge. Changes in channel capacity can be driven by changes to velocity or changes to the cross-sectional area of the channel. Velocity is altered by a change in slope (gradient) or a change in cross-sectional area and area is altered by either bed aggradation or degradation. The frequency of extreme floods over the last decade coupled with the amount of geomorphic change that has occurred in Spruce Woods Provincial Park has prompted investigation into whether channel capacity changes may be contributing to flood hazard. The method outlined by Slater et al. (2015) is applied to flow gauge measurements and associated field measurements of the Holland Gauging Station (Station 05MH005) to determine the drivers of flooding on the Assiniboine River (Chapter 3). This method uses daily discharge measurements of a gauging station to determine the change in flow frequency and field

measurements taken at the same gauging station to measure the change in channel capacity, cross-sectional area, and flow velocity that has occurred.

Studying the sedimentary products and morphological changes of extreme floods will refine point bar models and aid in the identification of extreme floods in the sedimentary record. Understanding what drives extreme floods will aid in predicting future flood events and what flood infrastructure might help mitigate the impact of these flood events.

1.2. Research Questions and Objectives

The main objective of this research is to i) understand the impact of extreme floods on sedimentary deposits, with special consideration of multiple extreme flood events, on the Assiniboine River, and ii) investigate factors that affect flood hazard and their relationship to the geomorphology and sedimentology of extreme flood events. More specifically, this research will connect geomorphic change that has occurred during extreme floods with the resultant sedimentology. It will also investigate whether geomorphic change of the channel is altering the flood hazard on the river. It is hypothesized that the sedimentary deposits of extreme floods on the Assiniboine River differ from annual deposits and that geomorphic change of the channel may be contributing to an increased frequency of extreme floods. The following questions will address the hypotheses of this research:

(1) Are deposits resulting from extreme floods distinguishable from deposits resulting from normal flows?

(2) What is the relative contribution of channel capacity to flood hazard on the Assiniboine River? Does geomorphic change (of the channel) contribute to a change in flood frequency?

Examining these questions will improve the understanding of the sedimentary deposits of extreme floods and provide insight into why these deposits occur. This will further refine sedimentary models of point bars and inform how to improve the prediction and mitigation of future floods in the region.

1.3. Research Organization

This thesis is organized into four chapters: chapter one is an introduction to the thesis topics, chapters two and three are compiled as standalone papers for the purpose of publication as peer-reviewed scientific articles, and chapter four addresses the overall conclusions and future work. The overarching subject of this thesis is quaternary fluvial geomorphology and sedimentology, with a focus on connecting geomorphic change to sedimentary deposits and alterations of flood hazard. This study analyzes a wide array of data utilizing both qualitative and quantitative methods. Chapter 2 presents detailed analysis of the sedimentary deposits of two point bars, using satellite imagery and LiDAR to constrain flood deposits. This includes identifying facies and vertical successions present and describing the mode of migration of the two point bars. Chapter 3 investigates the contribution of channel change to flood hazard. This is achieved using statistical modelling of field measurements and continuous flow gauge data from the Holland Gauging Station (Station 05MH005) conducted by the Water Survey of Canada. Finally, chapter 4 summarizes the results of chapters 2 and 3 and integrates them into an overview of extreme floods, their drivers, and impacts. This concluding chapter also address remaining questions and the opportunity for future work in this area.

1.4. Contribution of Authors

The general research question of this thesis was proposed by my thesis supervisor, Dr. Paul Durkin, based on my research interests. We collaborated on the design of the studies, and he aided in my literature review. I collected the data for this research with the assistance of my supervisor and four field assistants. I was responsible for data management and data analysis and received input and feedback from my supervisor. We outlined the structure of the two papers herein together; I conducted the literature search and wrote the chapters myself. I revised the thesis, implementing feedback from my supervisor and advisory committee – Dr. Zou Zou Kuzyk and Dr. Jens Ehn. I designed the figures with input from my supervisor and refined them with his feedback.

C.Morrow: conceptualization, research, methodology, investigation, analysis, data curation, writing original draft, writing, visualization, project administration; P. Durkin: funding acquisition, resources, conceptualization, research, methodology, investigation, analysis, supervision, review and editing, visualization review and editing; T.Ferens: investigation; L.Page: investigation; K.Mayo: investigation; J.Kroeker: investigation; Z.Kuzyk: writing review; J.Ehn: writing review.

1.5. References

Allen, J. R. (1965). A review of the origin and characteristics of recent alluvial sediments. *Sedimentology*, *5*(2), 89-191.

Bathurst, J. C., Thorne, C. R., & Hey, R. D. (1977). Direct measurements of secondary currents in river bends. *Nature*, *269*(5628), 504-506.

Blanckaert, K. (2010). Topographic steering, flow recirculation, velocity redistribution, and bed topography in sharp meander bends. *Water Resources Research 46*, 1-23.

Bluck, B. J. (1971). Sedimentation in the meandering River Endrick. *Scottish Journal of Geology, 7*(2), 93-138.

Bridge, J. S., Alexander, J. A. N., Collier, R. E. L., Gawthorpe, R. L., & Jarvis, J. (1995). Ground-penetrating radar and coring used to study the large-scale structure of point-bar deposits in three dimensions. *Sedimentology, 42*(6), 839-852.

Burge, L. M., & Smith, D. G. (1999). Confined meandering river eddy accretions: sedimentology, channel geometry and depositional processes. *Fluvial Sedimentology VI, 28*, 113-130.

Burn, D. H., & Whitfield, P. H. (2016). Changes in floods and flood regimes in Canada. *Canadian Water Resources Journal, 1*(1-2), 139-150.

Co-Operators. (n.d.*) How do we determine flood risk?* Retrieved August 2, 2022 from https://www.cooperators.ca/en/Resources/protect-what-matters/determining-flood-risk.aspx

Costa, J. E. (1974). Stratigraphic, morphologic, and pedologic evidence of large floods in humid environments. *Geology, 2*(6), 301-303.

Daniel, J. F. (1971). *Channel movement of meandering Indiana streams* (No. 732). US Government Printing Office.

Dietrich, W. E. (1987). Mechanics of flow and sediment transport in river bends. In *River channels: Environment and process* (Vol. 18, pp. 179-227). Oxford: Blackwell.

Fisk, L. H. (1974). Inverse grading as stratigraphic evidence of large floods: Comment. *Geology*, *2*(12), 613-614.

Gaur, A., Gaur, A., Yamazaki, D., & Simonovic, S. P. (2019) Flooding related consequences of climate change on Canadian cities and flow regulation infrastructure. *Water (Switzerland)*, *11*(1).

Ghinassi, M., Ielpi, A., Aldinucci., and Fustic, M., 2016, Downstream-migrating fluvial point bars in the rock record: *Sedimentary Geology*, *334*, 66-96.

Ghinassi, M., Moody, J., & Martin, D. (2018). Influence of extreme and annual floods on point-bar sedimentation: Inferences from Powder River, Montana, USA. *GSA Bulletin*, *131*(1-2), 71-83.

Hooke, R. L. B. (1975). Distribution of sediment transport and shear stress in a meander bend. *The Journal of geology*, *83*(5), 543-565.

Jackson, R. G. (1976). Depositional model of point bars in the lower Wabash River. *Journal of Sedimentary Research*, *46*(3), 579-594.

Kasvi, E., Vaaja, M., Alho, P., Hyyppä, H., Hyyppä, J., Kaartinen, H., & Kukko, A. (2013). Morphological changes on meander point bars associated with flow structure at different discharges. *Earth Surface Processes and Landforms*, *38*(6), 577-590.

Kasvi, E., Laamanen, L., Lotsari, E., & Alho, P. (2017). Flow patterns and morphological changes in a sandy meander bend during a flood—Spatially and temporally intensive ADCP measurement approach. *Water*, *9*(2), 106.

Knox, J. C. (1987). Stratigraphic evidence of large floods in the upper Mississippi Valley. *In Catastrophic flooding (pp. 155-180).* Routledge.

Leeder, M. R., & Bridges, P. H. (1975). Flow separation in meander bends. *Nature*, *253*(5490), 338-339.

Leopold, L.B., and Wolman, M.G. (1960) River meanders: Geological Society of America Bulletin, 71, p. 769–793

McGowen, J. H., & Garner, L. E. (1970). Physiographic features and stratification types of coarse-grained pointbars: modern and ancient examples 1. *Sedimentology*, *14*(1-2), 77-111.

Rasmussen, P. F. (2016) Assessing the impact of climate change on the frequency of floods in the Red River basin. *Canadian Water Resources Journal*, *41*(1–2), 331–342.

Simonovic, S. P., & Li, L. (2004) Sensitivity of the Red River Basin Flood Protection System to Climate Variability and Change. In *Water Resources Management* (Vol. 18).

Slater, L. J., Singer, M. B., & Kirchner, J. W. (2015) Hydrologic versus geomorphic drivers of trends in flood hazard. *Geophysical Research Letters*, *42*(2), 370–376.

Shrubsole, D., Brooks, G., Halliday, R., Haque, E., Kumar, A., Lacrois, J., Raisd, H., Rousselle, J., and Simonovic, S. P. (2003) An Assessment of Flood Risk Management in Canada. *Institute for Catastrophic Loss*

Smith, D. G., Hubbard, S. M., Leckie, D. A., & Fustic, M. (2009). Counter point bar deposits: lithofacies and reservoir significance in the meandering modern Peace River and ancient McMurray Formation, Alberta, Canada. *Sedimentology*, *56*(6), 1655-1669.

CHAPTER TWO:

THE SEDIMENTOLOGICAL AND GEOMORPHOLOGICAL IMPACT OF THREE HIGH-MAGNITUDE FLOODS ON THE ASSINIBOINE RIVER, SOUTHWESTERN MANITOBA, CANADA

2.1. Introduction

The geomorphic changes caused by extreme floods and the extent to which they are preserved in the sedimentary record has received considerable interest since the 1960s (e.g. Wolman and Miller, 1960; Costa, 1974a; Wolman & Gerson, 1978 Gupta, 1983). An extreme flood is defined as one with a recurrence interval greater than or equal to 100 years (Kundzewicz et al., 2013). The extent of geomorphic change caused by extreme floods is controlled by several factors, including river planform (Hickin & Sichingabula, 1988; Miller, 1990), degree of channel confinement (Baker, 1977; Nanson, 1986), suspended sediment concentration (Magilligan, 1998), and character of alluvial deposits (Stewart & LaMarche, 1967; Nanson, 1986; Magilligan, 1998). Studies have demonstrated little lasting impact on river geomorphology (Wolman & Eiler, 1958; Gardner, 1977; Gomez et al., 1995; Magilligan et al., 1998; Heitmuller et al., 2017), extensive erosion and deposition (Stewart & LaMarche, 1967; Nanson, 1986), and a combination of significant to negligible geomorphic change within the same basin during a single flood event (Hickin & Sichingabula, 1988; Miller 1990). While extreme floods have the potential to significantly alter a river's morphology (e.g., Magilligan et al., 2015), the few studies completed on sedimentary deposits of extreme floods on meandering rivers have found that the sedimentary record of extreme floods is not distinct from that of annual floods (e.g. Gomez et al., 1995; Heitmuller et al., 2017).

Geomorphic change and point-bar deposits are intrinsically connected as meandering rivers migrate laterally through concurrent erosional and depositional processes. As the outer bank is eroded, deposition occurs along the inner bank, which leads to the formation of point bars (Leopold and Wolman, 1960). Meander bends develop a unique three-dimensional (3D) flow structure that is characterized by secondary helical circulation and flow separation that

develops downstream of the bend apex (Hooke, 1975; Leeder & Bridges, 1975). This secondary helical circulation results in a bottom current moving up the slope of the point bar, sorting the sediment such that coarser grained sediment is deposited at the base of the point bar and finer sediment is deposited at the top of the point bar (Dietrich et al., 1979). This results in an overall upward-fining trend that is documented in most facies models of a point-bar deposit (e.g. Allen, 1965a; McGowen & Garner, 1970; Bluck, 1971). Although the flow structure and resulting deposits of a meandering river are relatively well understood, recent research has highlighted how variable discharge alters this flow structure and therefore can affect the resulting deposits (Kasvi et al., 2013; 2017; Ghinassi et al., 2018).

The deposits associated with extreme floods in sandy meandering rivers have been characterized in several studies (Costa, 1974b; Fisk, 1974; Knox, 1987). These studies have found that while flood deposits may have the typical fining-upward trend of point bars (Allen, 1970), they may also display coarsening-upward trends that are atypical (Costa, 1974b; Fisk, 1974; Knox, 1987). However, studies on the deposits of multiple extreme floods are lacking, likely due to the rarity of such events over human timescales. Studies that investigate multiple extreme floods are typically numerical models, with a focus on channel geometry and the resulting flood hazard (Guan et al., 2016; Tu et al., 2017). Based on predictions of future climate regimes, climate change has the potential to significantly alter human exposure to flood hazard; however, these predictions have a large degree of variability due to different projections of regional changes in climate (Arnell and Gosling, 2016). For instance, based on 21 different climate models, the range of exposure of people and cropland in 2050 to a doubling of flood frequency and changes in flood risk varies from -9% to 376% (Arnell and Gosling, 2016). Thus, understanding the effects of multiple extreme flood events on river migration and the resulting

sediment erosion and deposition is important for predicting the impact on surrounding infrastructure and human lives.

An opportunity to evaluate the geomorphic change and associated deposition caused by multiple extreme floods has arisen in the last decade along the Assiniboine River in southwestern Manitoba. The Assiniboine River is a sand-and-gravel meandering river that experienced three >250-year recurrence-interval floods in 2011, 2014, and 2017, resulting in a meander-bend cut off and significant erosion and sediment deposition along two meander bends in Spruce Woods Provincial Park. The purpose of this study is to investigate the erosion and deposition that has occurred during these extreme flood events with the goal of developing criteria to identify multiple extreme floods in the stratigraphic record and predict the impact of future flood events. This is achieved by using satellite imagery, LiDAR, remotely piloted aircraft system structure from motion (RPAS-SfM) photogrammetric models of the study area, sediment sampling, and excavated trenches to quantify areas of sediment deposition or erosion and characterize the sedimentology and stratal architecture of multiple extreme flood deposits. The results from this study inform the identification of extreme floods in the sediment record and improve reconstructions of past environments and their hydrologic cycles. Furthermore, improving our understanding of how future extreme floods will alter the sedimentology of the region may help guide local flood mitigation infrastructure.

2.2. Background and Study Area

The Assiniboine River valley was formed by glacial meltwater and drainage of proglacial lakes during deglaciation approximately 12,000 years ago (Klassen, 1972). The eastward flowing river can be divided into the upper and lower Assiniboine River, which are

located upstream and downstream of Portage la Prairie, Manitoba, respectively (Fig. 2.1) The upper portion of the river valley erodes into sediment from the late glacial Assiniboine Delta, forming a deep, confining valley (Fenton, 1970; Kehew and Teller, 1994; Boyd, 2007). The lower portion of the river erodes into the flat lakebed of glacial Lake Agassiz where it has an especially gentle slope of 5×10^{-4} (Rannie et al., 1989; Blais et al., 2016a), eventually connecting with the northward flowing Red River in downtown Winnipeg, Manitoba.

Manitoba has a long history of flooding, with the largest flooding event on record dating back to the 1826 Red River Flood (Blais et al., 2016a). More recently, the 1950 and 1997 Red River floods prompted early flood mitigation efforts along the Red River's largest tributary, the Assiniboine River, such as the Shellmouth dam and the Portage Diversion along the Assiniboine River's upper reaches (Blais et al., 2016a). Flooding continues to be a problem in the province, particularly along the lower Assiniboine River, where the particularly low slope and meandering nature of the river reduces channel conveyance capacity (Blais et al., 2016a).

Over the last decade, the Assiniboine River has experienced two >100-year recurrence interval floods and an extreme flood stage event (Fig. 2.2). In 2011, the Assiniboine River experienced its largest flood recorded over the 100-year period during which records were kept for the river (Blais et al., 2016b). This unprecedented flood was caused by several contributing factors, starting with extreme antecedent soil moisture, followed by high winter snowpack and unprecedented spring rainfall (Government of Manitoba, 2013; Blais et al., 2016b). During the flood, peak discharge reached 1460 m^3/s, exceeding the flood stage discharge of 970 m^3/s, and flooding persisted for 120 days (GOM, 2013; Blais et al., 2016b). The 2011 flood was estimated to have a return period of 350 years, however, only three years later the Assiniboine flooded once again with a similar peak discharge (Ahmari et al., 2016). The 2014 flood was

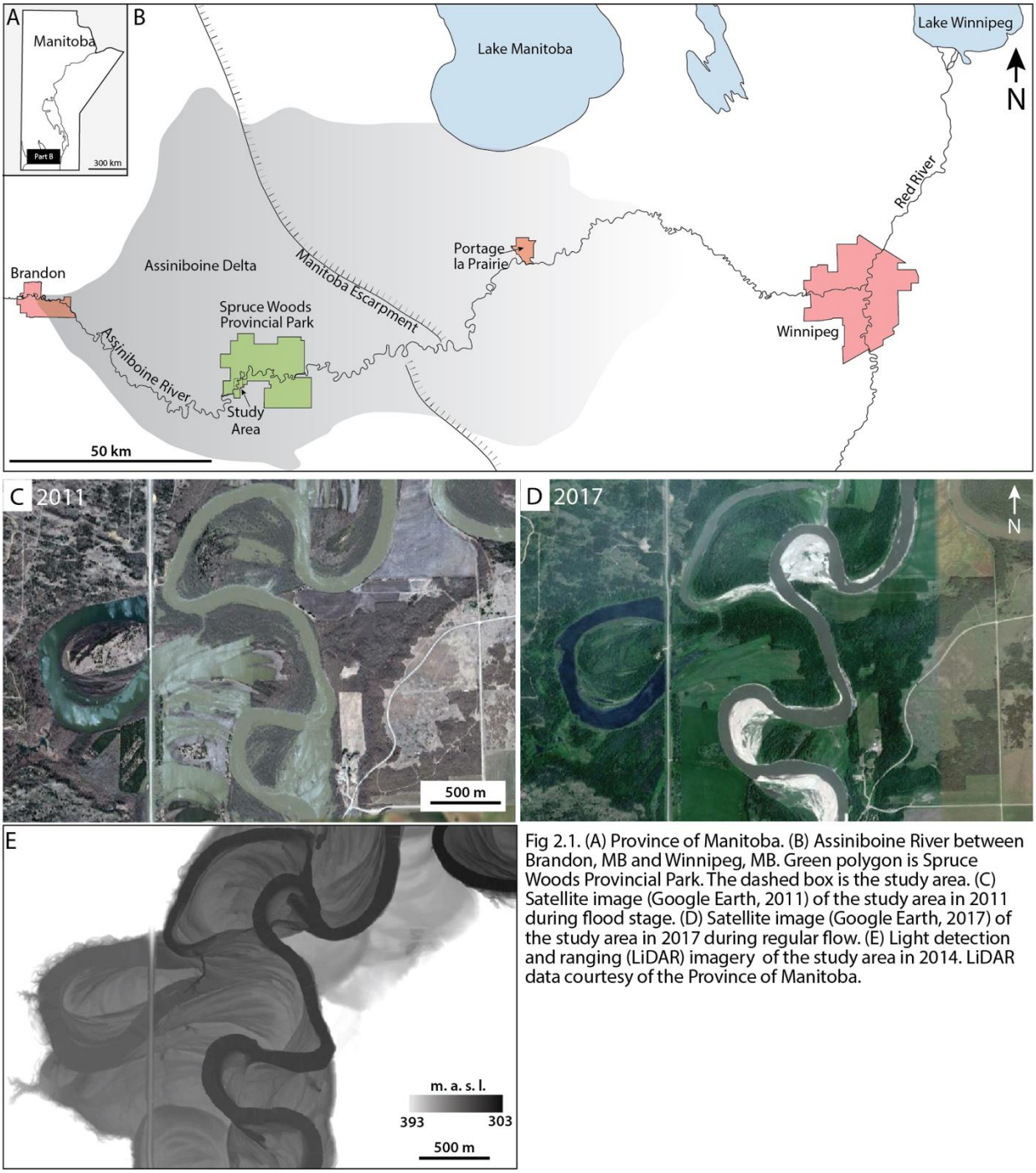

Fig 2.1. (A) Province of Manitoba. (B) Assiniboine River between Brandon, MB and Winnipeg, MB. Green polygon is Spruce Woods Provincial Park. The dashed box is the study area. (C) Satellite image (Google Earth, 2011) of the study area in 2011 during flood stage. (D) Satellite image (Google Earth, 2017) of the study area in 2017 during regular flow. (E) Light detection and ranging (LiDAR) imagery of the study area in 2014. LiDAR data courtesy of the Province of Manitoba.

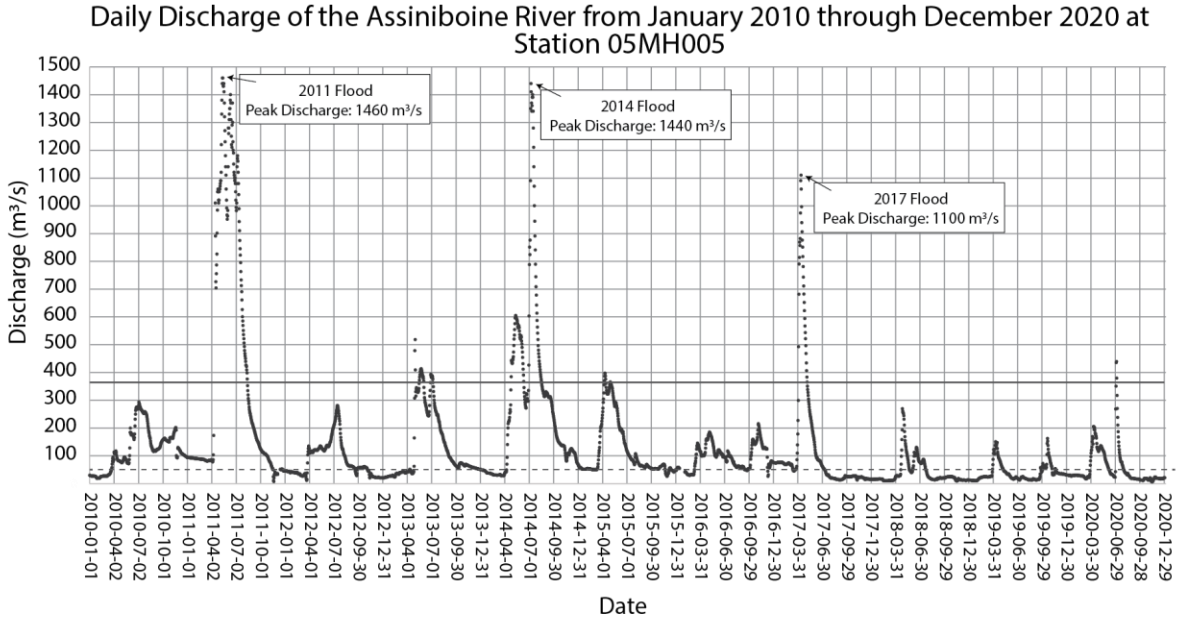

Fig 2.2. Daily discharge (black circles) of the Assiniboine River at Holland Gauging Station (Station 05MH005), 45 km downstream from the study area. Baseflow (56 m³/s) is indicated by the dashed line and moderate flood stage (364 m³/s) is indicated by the solid line.

unprecedented as it was a summer flood whereas historically the Assiniboine River had only flooded in the spring (Ahmari et al., 2016). The 2014 flood was caused by extreme summer rainfall on an already saturated drainage basin (Ahmari et al., 2016). It had a peak discharge of 1440 m^3/s and was calculated to have a return period of approximately 250 years (Ahmari et al., 2016). The Assiniboine River once again experienced an extreme discharge in 2017, with peak discharge reaching 1100 m^3/s albeit the discharge did not persist for as long as the previous two events.

The study area is in Spruce Woods Provincial Park (SWPP), southwestern Manitoba. The study area covers approximately 4.4 km^2 of the Assiniboine River channel belt and over this distance the river is an average of 60 m wide and 3.5 m deep with a sinuosity of 2.54. The baseflow, taken from the nearest gauging station 40 km downstream at Holland, MB, is 46 to 53 m^3/s and bank full discharge is 736 m^3/s (Government of Manitoba, 2021). Although continuous suspended sediment discharge is not available at the gauging station, former studies on sediment load in the Assiniboine River reported the highest concentration of sediment occurs in the study area (Ashmore, 1992). At the study site, the Assiniboine River's drainage basin is 160 000 km^2, or almost 99% of the total drainage basin (Brimelow et al., 2015). Peak discharge typically occurs in April or May, and occasionally in July. The Assiniboine River has a valley width to channel width ratio of 18:1, which is classified as first-degree confinement where the river channel is only in intermittent contact with the valley walls (e.g., Lewin and Brindle, 1977; Nicoll & Hickin, 2010).

Two meander bends and their associated point bars near the Kiche Manitou campground east of provincial highway 5 (Fig. 2.1), were selected due to their accessibility and significant change over the last decade. The WRPB is 310 m long and 450 m wide, covering approximately

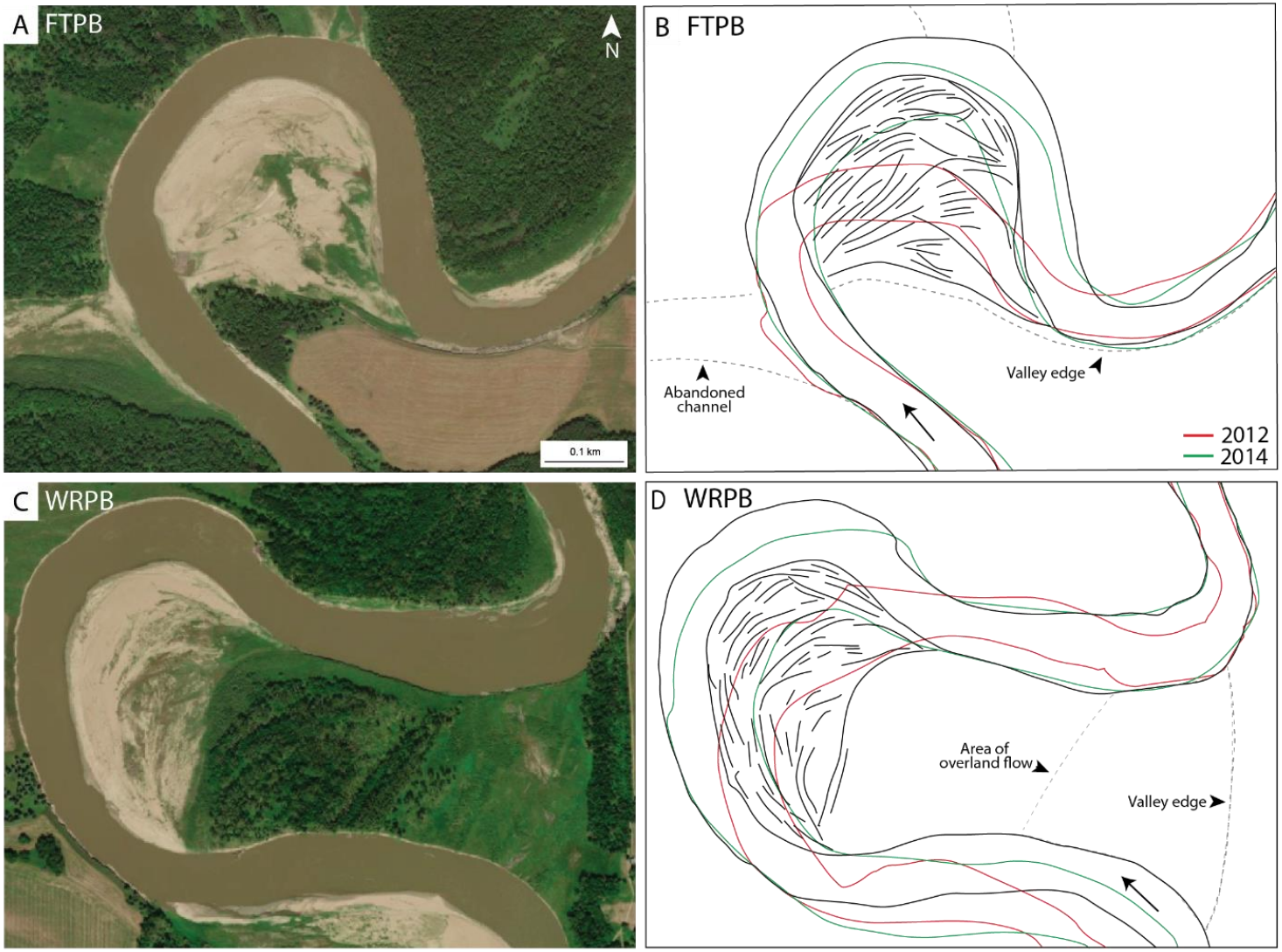

Fig 2.3. (A) Satellite image of the FTPB (Esri, 2018). (B) Trace of the FTPB. The position of the channel in 2012 and 2014 are traced in red and green, respectively. (C) Satellite image of the WRPB (Esri, 2018). (D) Trace of the WRPB. The area of overland flow is marked by the grey dashed polygon.

0.14 km^2. The Fallen Tree Point Bar (FTPB) is 360 m long and 400 m wide, covering an area of approximately 0.15 km^2 (Fig. 2.3). At the study area, the river
bedload consists mainly of sand and gravel sourced locally as the river cuts into the Assiniboine Delta and glacial till deposits (Rannie et al., 1989). While the gauging station used in this study does not record sediment load, a study by Ashmore (1990) on the suspended load of the Assiniboine River documented a significant increase by a factor of 40 between Russel, Manitoba and Holland, Manitoba. Wolowich (1985) reported the mean grain size of the sediment load at Holland, Manitoba as fine-to-coarse sand. The river has been anthropologically altered just upstream of the study area by limestone riprap that was installed following the 2014 flood to protect local roads from cutbank erosion.

2.3. Methods

This study utilizes a combination of remotely sensed and field-based data to quantify the geomorphic and sedimentary change of two point bars over the course of a decade. Annual satellite imagery between 2010 and 2020 was used to quantify the geomorphic change at WRPB and FTPB (Planet Team, 2017). Images from Planet Labs Inc. have a resolution of 3 m/pixel. Photos were georeferenced using ArcGIS 10 with local roads used as ground control points. These images were used to quantify the amount of deposition that occurred on the point bar and the extent of outer bank retreat during channel migration. Yearly manual measurements included the area deposited on the point bar, the area eroded from the cutbank, and the length of lateral migration along the point bar axis. Additionally, geomorphic measurements such as amplitude, path length, sinuosity, and bend curvature were measured from satellite imagery (Fig. 2.4.). Amplitude (A) is the lateral extent of a meander bend, measured as the lateral distance between

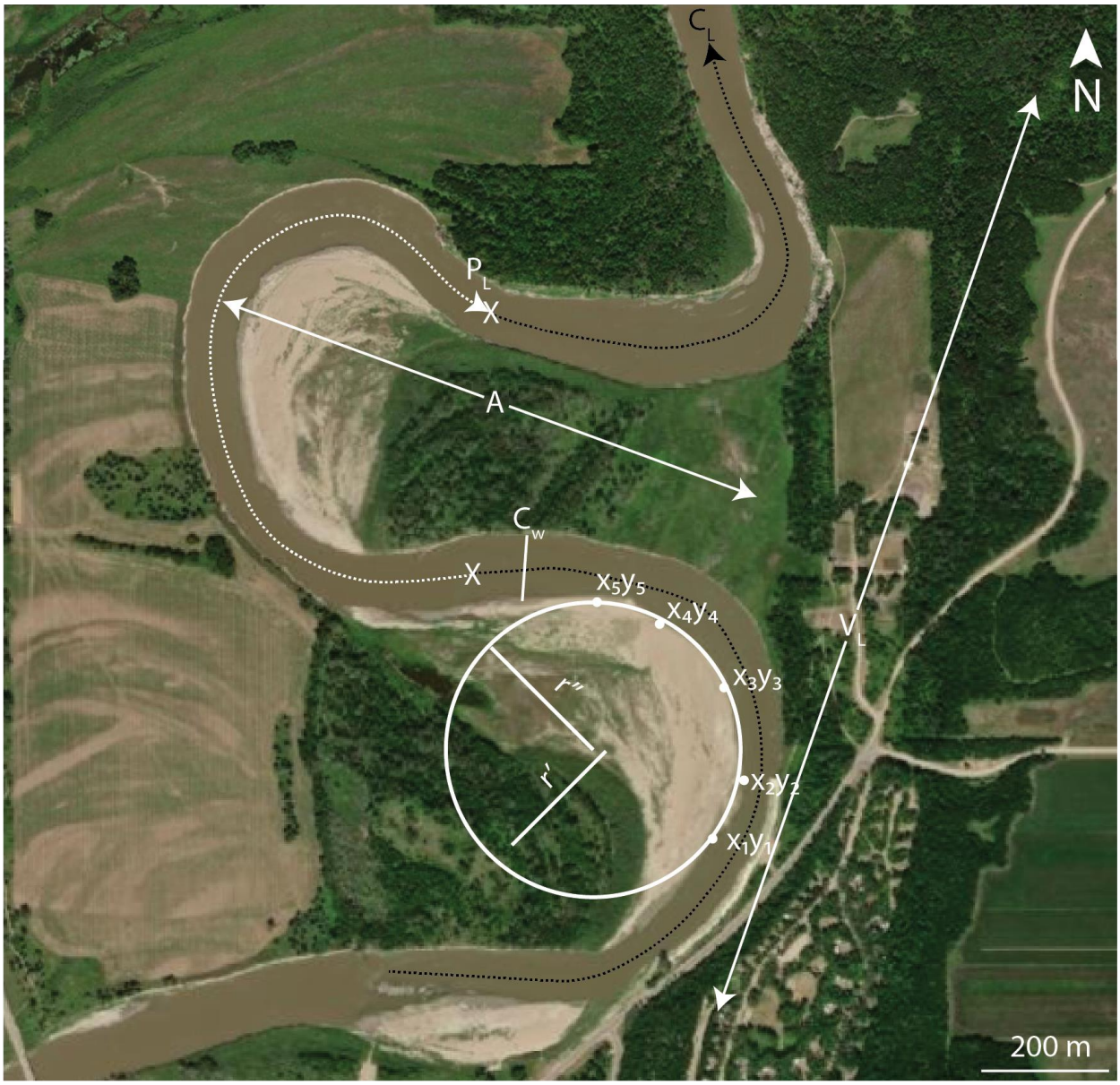

Fig 2.4. Parameters of meander bends. The satellite image (Esri, 2018) is centered on the WRPB and the preceding meander bend. V_L is valley length. P_L is path length from inflection point (X) to inflection point (X). C_w is the channel width at a straight section of the channel. A is amplitude, measured from the channel centre line to the centre line of the preceding bend. r′ is the radius of a circle that crosses through x_2y_2, x_3y_3, and x_4,y_4. r″ is the radius of a circle that crosses through x_1y_1, x_3y_3, x_5y_5. Each x_ny_n point is placed one C_w apart and x_3y_3 is the bend apex.

the centreline of two successive meander bends (Leopold, Wolman & Willer, 1964). The path length (P_L) is the length of the channel from one inflection point to a succeeding inflection point, a measurement of the channel length of one meander bend (i.e. ½ wavelength). Sinuosity (S) is a measure of the degree of complexity or curvilinearity of a meandering channel (Andrle, 1996). Sinuosity is commonly measured as the ratio between the length along the centreline of a channel (L_c) to the length of the valley (L_v) over a given reach. A light detection and ranging (LiDAR) survey from late 2014 (Government of Manitoba, 2014) was used to measure a series of topographic profiles of the point bars, which allowed for division of vertical sequences of sediment into pre-2014 and post-2014 deposits. A digital surface model (DSM) of each point bar was rendered from a RPAS-SfM model collected in the summer of 2020 using Pix4Dmapper software (Turner et al., 2012). A second series of topographic profiles for each point bar was measured using the RPAS-SfM DSM to compare with the 2014 profiles.

A total of 31 trenches was manually excavated in 2020 and 2021 to characterize the internal sedimentology of the point bars (Fig. 2.5). The trenches were between 0.5 to 2 m in depth and 0.5 m to 7 m in width. The deposits were analyzed using classical field methods to detail sedimentary structures, grain size, bed and cross-set thickness, and paleoflow direction. Grain size diameters were measured in the field using a hand lens and grain-size card. Field measurements in combination with field photos were used to produce a facies scheme consisting of five distinct facies classified based on sedimentary structures, grain size, and bedding characteristics. Surface grain size measurements were collected from the surface of the point bar. These grain size measurements were plotted on satellite imagery to visualize point-bar surface grain size distribution and trends.

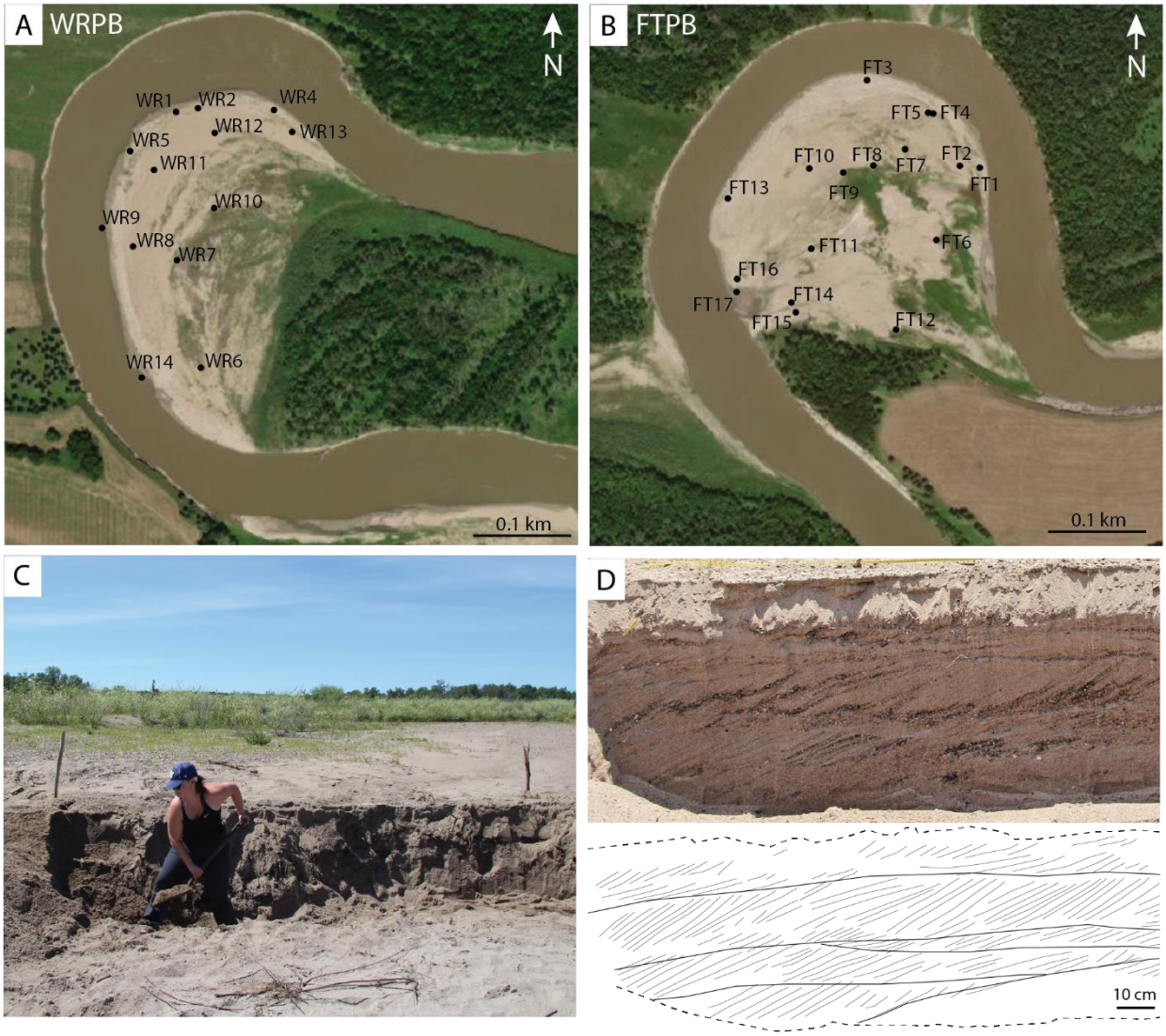

Fig 2.5. (A) Satellite image of WRPB in 2018 (Esri, 2018) with all 13 trench locations marked. (B) Satellite image of FTPB in 2018 (Esri, 2018) with all 17 trench locations marked. (C) Trench (WR2) in the process of being excavated. It is approximately 5 m wide and 1 m deep. (D) WR2 following excavation, with trace of sedimentary features below.

.

2.4. Results and Analysis

Five recurring facies are identified from the excavated trenches (Fig. 2.6) and summarized in Table 1. The facies comprise three vertical sequences (Fig. 2.7) that are described in the context of the two topographic profiles (Fig. 2.8; Fig. 2.11). Satellite imagery is used to measure the geomorphic change that has occurred over the past decade (Fig. 2.14; Fig. 2.15), summarized in Table 2. Surface grain size measurements from WRPB characterize grain-size distribution on the point bar.

2.4.1. Facies

Facies 1: Cross-stratified gravels

Facies 1 (F1) is characterized by cross-stratified, matrix-to-clast-supported granule-to-pebble gravel with a medium-to-very coarse-grained sand matrix. F1 occurs in both point bars of interest, typically upstream of their bend apices at the time of deposition (Fig. 2.6a). The grain size of the gravel ranges from granule to cobble; the sand is medium-to-coarse-grained and poorly sorted. Tabular and trough cross-stratification are the sedimentary structures and cross sets range from 10 to 70 cm thick. The foresets are normally graded and measure from 1 to 5 cm thick. The F1 beds range from 20 to 70 cm in thickness and have sharp upper and lower contacts.

Facies 1 is associated with high-energy deposition on the upstream portion of the upper- and lower-point bar and channel thalweg. The migration of sandy-gravel dunes requires sufficiently high-discharge with sufficient depth to transport coarse sediment and drive the migration of bedforms. The normal grading seen in the foresets is the result of alternating

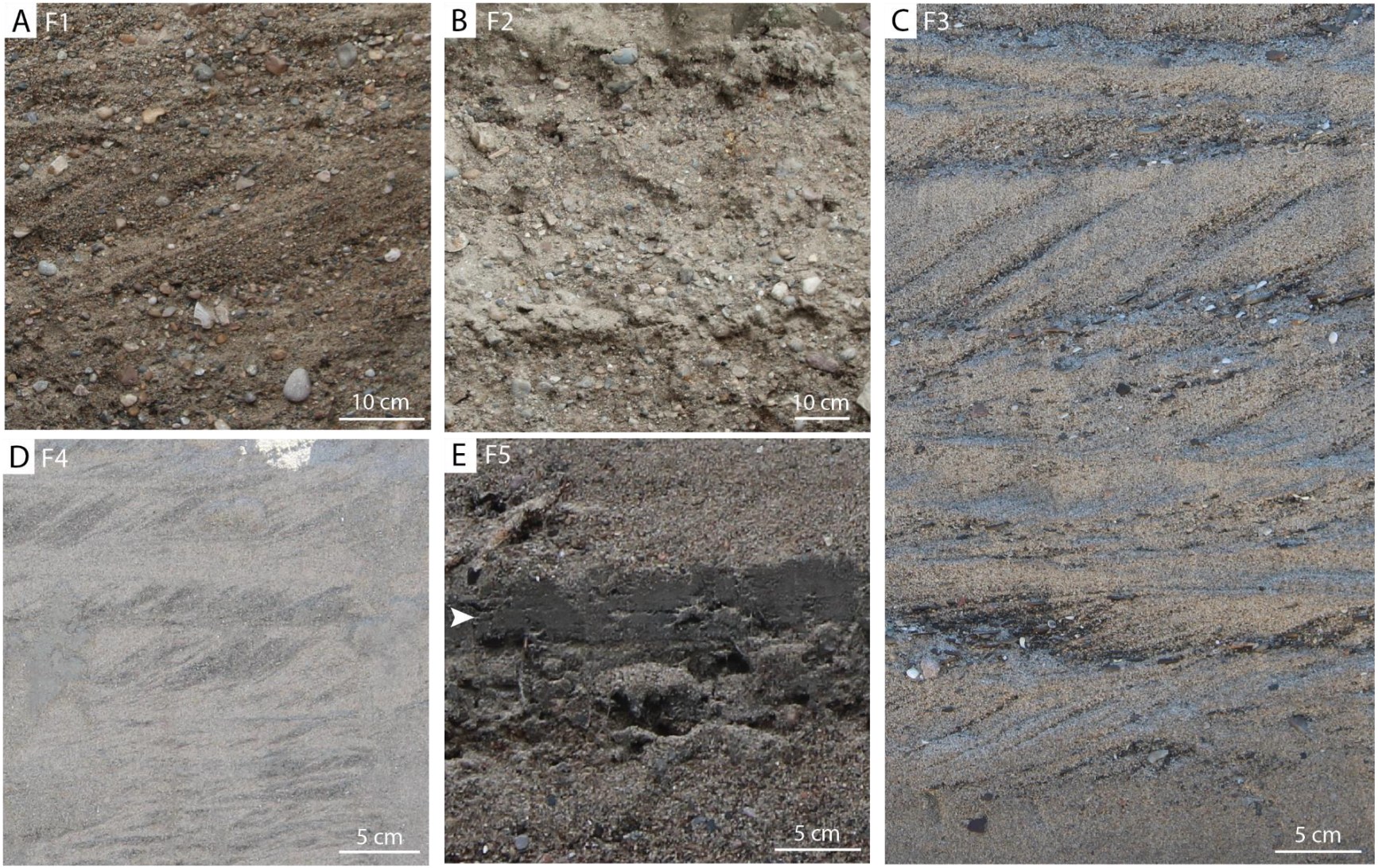

Fig 2.6. Facies of the Assiniboine River point bar deposit. (A) Facies 1: Cross-stratified gravels. (B) Facies 2: Massive gravels. (C) Facies 3: Cross-stratified medium-to-coarse sand. (D) Facies 4: Cross-stratified fine sand. (E) Facies 5: Mud.

avalanching of coarser-grained sediments on the lee-side followed by the avalanching of finer-grained sediments (Allen, 1965b; Smith, 1972; Jablonski & Dalrymple, 2016). Coarse-grained trough cross-stratification is associated with the migration of three-dimensional dunes in the deeper portion of the channel, such as the thalweg (Miall, 1985). Coarse-grained tabular cross-stratification is the migration of two-dimensional dunes atop of the point bar or along the flank of the point bar during floods (Miall, 1985). The occurrence of F1 on the upstream portion of the point bars is consistent with the expected grain size trends around a meander bend (e.g. Nanson, 1980; Bridge et al., 1995).

Facies 2: Massive gravels

Facies 2 (F2) consists of poorly sorted gravels with no discernible sedimentary structure (Fig. 2.6b). This facies occurs in both point bars, exclusively in the upstream portion of the point bar. Clasts are mainly pebble-to-cobble sized and the matrix is composed of medium-upper to very coarse lower sand. Overall bed thickness ranges from 20 to 80 cm with sharp upper and lower contacts.

Massive deposits, such as F2, are caused by rapid deposition that inhibits the formation of sedimentary structures (Leeder, 2011). This facies is the result of a rapid decrease in energy during a high-energy flow event, such as an extreme flood, on the lower point bar and channel thalweg.

Facies 3: Cross-stratified medium-to-coarse sand

Facies 3 (F3) is characterized by cross-stratified medium- to very coarse-grained cross-stratified sand. It is the most common facies, occurring throughout both point bars of interest

(Fig. 2.6c). The grain size ranges from medium-lower to very coarse-upper sand and is moderately to poorly sorted. Granule to pebble size clasts are commonly present at the base of cross sets and decrease in frequency upwards in a bed. The thickness of beds ranges from 15 to 50 cm, and they typically have sharp upper and lower contacts. Sedimentary structures are low- to high-angle tabular cross stratification (Fig. 2.6c). Foresets range from 1 to 3 cm in thickness and are commonly normally graded. Cross sets range from 3 to 40 cm and decrease in thickness upward.

Facies 3 is associated with moderate- to high- energy deposition on the middle to upper point bar surface. Sandy tabular cross-stratification is the result of either transverse two-dimensional dune migration or sand waves during moderate flow and is confined to shallower water depths such as the flank of the point bar (Miall, 1985). The coarser grained clasts are preserved in the dune troughs (Bridge et al., 1995). The graded foresets are indicative of intermittent avalanching of coarse-grained sediments followed by finer materials.

Facies 4: Cross-stratified fine sand

Facies 4 (F4) is characterized by cross-stratified fine-grained sand (Fig. 2.6d). F4 occurs in both studied point bars, commonly downstream of their bend apices at the time of deposition. The grain size ranges from fine-lower to fine-upper sand and is moderately to well sorted. Granules are present at the base of cross sets and become less common upward within a bed. Sedimentary structures are exclusively low- to high-angle tabular cross stratification (Fig. 2.6d). Cross sets range in thickness from 1 to 5 cm and decrease in thickness upward. Overall bed thickness ranges from 10 to 40 cm. Foresets are usually less than 1 cm thick with local mud drapes. The base of beds and cross sets are sharp, while the top is gradational into F1 or sharp.

Facies 4 is associated with moderate- to high-energy deposition on the downstream portion of the middle to upper point bar surface. Tabular cross stratification is a result of subaqueous straight-crested dunes migrating during high-discharge flows (Miall, 2010). Granules are preserved exclusively in the dune trough (Bridge et al., 1995). Local mud drapes reflect waning flow conditions and fine-grained deposition. Subsequent dune migration does not entirely rework or remove mud drapes and could reflect subtle fluctuations in flow discharge throughout a flood cycle. The prevalence of F4 on the downstream portion of the studied point bars is consistent with downstream grain-size fining around meander bends (e.g., Nanson, 1980; Bridge et al., 1995).

Facies 5: Mud

Facies 5 (F5) consists of massive and faintly laminated silt-and-clay-sized sediment (Fig. 2.6e). F5 occurs in both point bars of interest, typically downstream of their bend apices at the time of deposition. The grain size is clayey-silt mud and it is well sorted. The mud beds are typically thin, on average 3 cm thick; however, they can measure up to 10 cm. The upper contacts of the beds are sharp, whereas the base contacts are gradational into F2 or sharp.

Facies 5 is associated with low-energy deposition on the downstream portion of the upper point bar surface. Classically, mud deposits have been interpreted to have settled from suspension, coming from slack water on bar tops or overbank during floods (Church, 2006). Recent research has found, however, that mud deposition may also occur as a result of sand-sized mud aggregates being transported as suspended bedload material (Lamb et al., 2020).

2.4.2. Vertical Successions

Vertical successions were determined from trenches excavated on the point bar to characterize vertical variations in sedimentation. Three unique vertical successions were identified: i. fining-upward, ii. Coarsening-upward, and iii. Consistent grain size.

The fining-upward successions in the study area are typically represented by F3 deposits overlain by F4 and F5 deposits (Fig. 2.7a). This observation is typical of point-bar deposits and widely described in depositional models (e.g. Allen, 1970; Bluck, 1971). The fining-upward vertical trend is a Waltherian result of the grain-size fining from the channel thalweg to top of the point bar and the downstream fining from the bar head to bar tail (Allen, 1970; Bluck, 1971). Both trends arise from the secondary helical flow structure in a curved channel. Under fully developed secondary flow, coarser sediment is deposited in the channel thalweg and finer sediment is deposited on the bar top due to change in water depth and radial distance along the slope of the point bar (Dietrich et al., 1979; Allen, 1982). Secondary helical flow around the point bar also sorts the sediment from the bar head to bar tail. As flow enters the bend, the high velocity core (HVC) is located near the convex bank of the channel and gradually shifts towards the concave bank along the bend due to the point bar and bend curvature (Hooke, 1975; Bridge & Jarvis, 1976; Dietrich & Smith, 1983; Dietrich & smooth, 1984). As the HVC shifts from the point bar to the cutbank, maximum stream power and sediment transport shift to the cutbank as well. The lower velocities and a recirculation zone downstream of the bend apex results in the deposition of fine material over the point-bar tail (Bridge & Jarvis, 1976). As the point bar migrates laterally, an upward-fining lateral accretion deposit records the transition from channel, to point bar, to floodplain (Allen, 1970).

A coarsening-upward succession consists of F3 and F4 overlain by either F1 or F2 (Fig. 2.7c). While this succession is not included in typical models of point bars, it has been

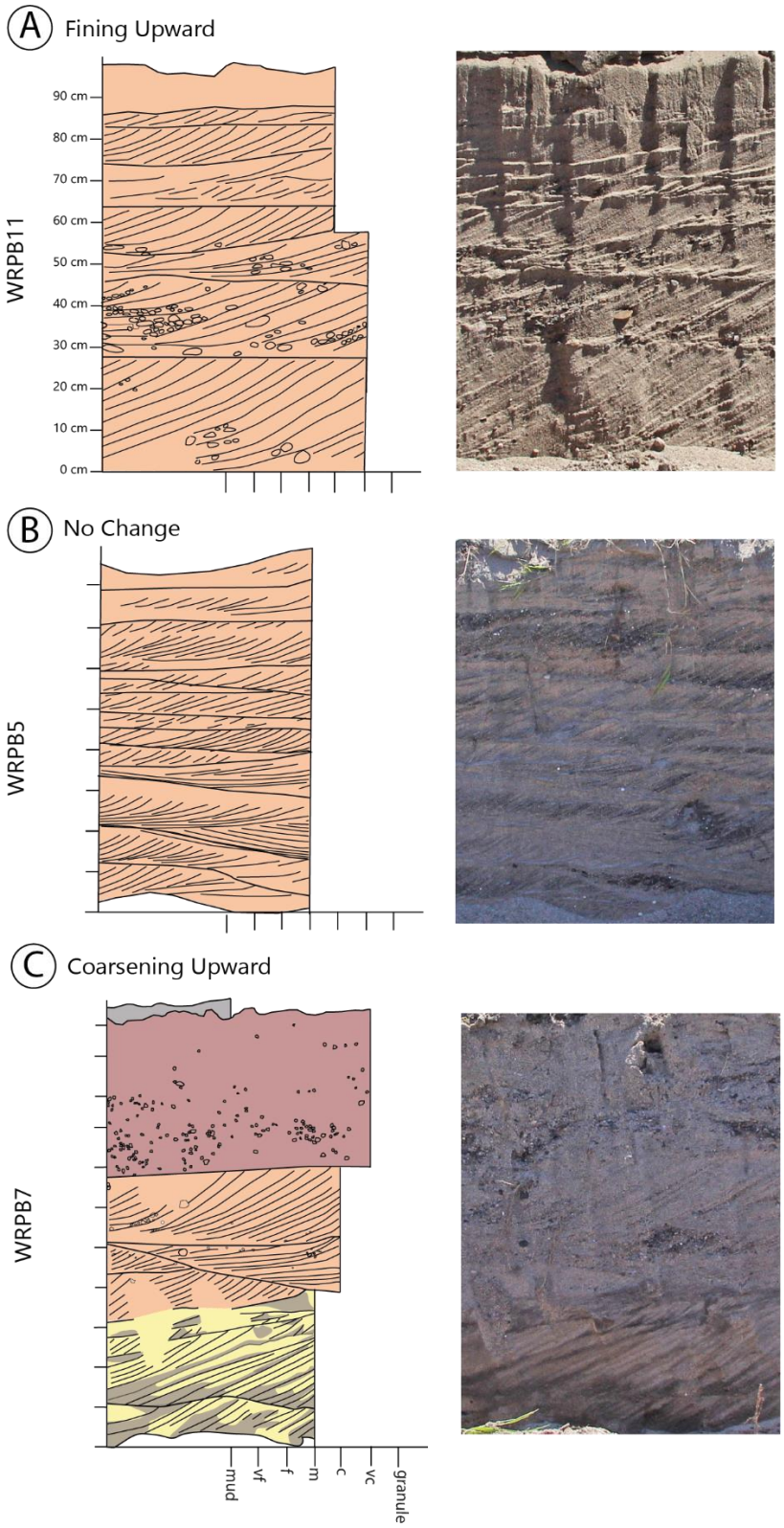

Fig 2.7. Vertical succesions measured from trenches. (A) Fining-upwards succession. Mean grain size decreases upwards; typical point bar facies. (B) No change in vertical trend. Mean grain-size is consistent throughout; this succession has not undergone sufficient aggradation to be a complete succession.(C) Coarsening-upwards succession. Mean grain size increases upwards; associated with extreme floods.

identified in studies of extreme flood events (e.g., Knox, 1987). These deposits are attributed to high-magnitude flood events with sufficient energy to drive flow over the point bar head (Dietrich and Smith, 1983). This changes the dynamics of the flow, spreading the conditions present at the entrance to the bend further downstream to the central zone of the point bar (Ghinassi et al., 2018). Secondary circulation is restricted to the downstream portion of the point bar, or may even be non-existent (Kasvi et al, 2013; Ghinassi et al., 2018). As the conditions that cause coarser sediments to be deposited on the point spread downstream, they over-lie the finer material that had previously been deposited by normal flows, resulting in the coarsening-upward succession illustrated here.

The vertical sequences that do not display any grading are mostly represented by F3 (Fig. 2.7c). These sequences are located close to the active channel and were deposited during the last extreme flood in 2017 and normal flows in 2015 and 2019. As no further accretion has occurred since their deposition, the location has not aggraded to the same extent as the other successions and is therefore still incomplete (Fig. 2.14; Fig. 2.15). The complete vertical succession in these locations will depend on the nature of future flood events and continued point bar migration.

2.4.3. Point Bar Architecture

Cross sections of the point bars were constructed in ArcGIS Pro to visualize the change that has occurred between 2014 and 2020, utilizing the 2014 DEM and 2020 DSM. From these cross sections, approximate measurements of the area of sediment that had been deposited and eroded along the cross section were made. Furthermore, the deposits that had been exposed through excavation could be separated into deposits associated with the 2014 extreme floods and deposits that occurred in subsequent years. As there is no topographic data available prior to

2014, it is assumed that anything below the 2014 profile is the result of deposition during or after the 2011 flood.

Cross section a-a' of the WRPB is the furthest upstream; the point bar has migrated approximately 70 m and the cross-sectional area of sediment deposited along this cross section is approximately 400 m^2 (Fig. 2.8). The 2014 profile of the point bar has a steeper slope of nearly 30° towards the channel compared with the 2020 slope of approximately 14°.Additionally, the 2014 scroll bars are more exaggerated, the ridges have higher amplitude, and the swales erode deeper into the point bar. Along the 2020 topographic profile there are three trenches – WR7, WR8, and WR9. The two trenches closest to the active channel, WR9 and WR8, do not overlap with the 2014 topographic profile and both display the typical fining upward trend where F1 deposits are overlain by F3 deposits (Fig. 2.9). The trench furthest from the active channel intersects deposits the 2014 profile and has a coarsening-upward trend. At the base of the trench is a 30 cm-thick F4 deposit followed by a 35 cm-thick F3 deposit, then succeeded by a 40 cm-thick F2 bed. The trench is capped at the top by a thin 5 cm-thick bed of F5 (Fig. 2.9).

The second cross section from WRPB, b-b', is close to the bend apex where the point bar has laterally accreted approximately 70 m, and the area of sediment deposited along this cross section is approximately 410 m^2 (Fig. 2.8). The 2014 topographic profile has an average dip angle of 12° and the 2020 profile has an average dip angle of 22 °. The 2014 profile has more ridge-and-swale couplets indicating scroll bars whereas the 2020 profile has ridges that lack the associated swales in between scroll bars. The trenches along this transect have a similar trend to that of the previous cross section. The trench closest to the active channel, WR5, is 85 cm deep and is entirely F3 deposits and does not display any distinct grain size trend (Fig. 2.9). The

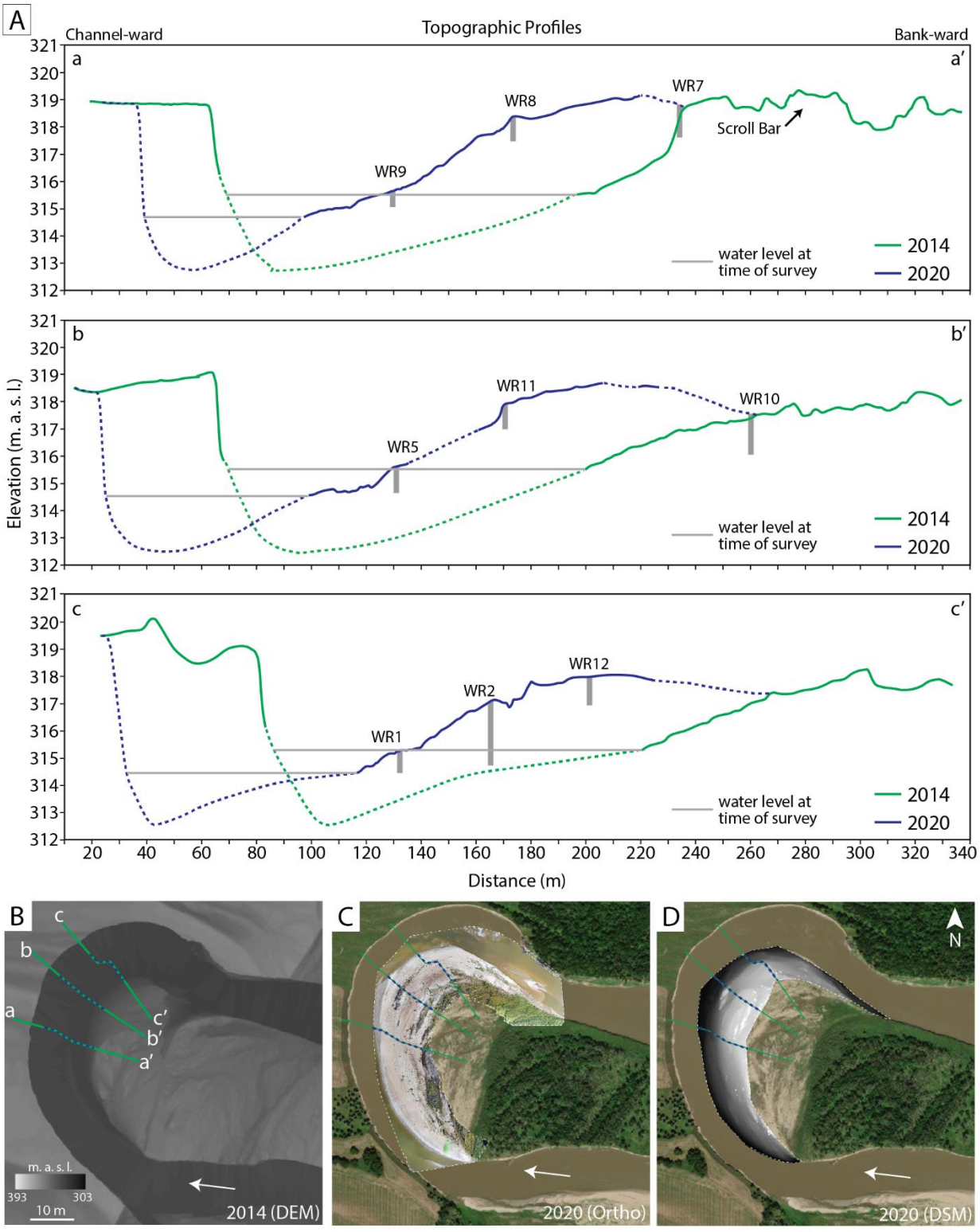

Fig 2.8. (A) Cross-sectional profiles of the WRPB. The 2014 profile (green solid line) is constructed from a DEM rendered from LiDAR captured fall 2014, post-2014 summer flood. The 2020 (blue solid line) profile is constructed from a DSM rendered from a RPAS-SfM model from summer 2020. Dashed lines indicate extrapolated surfaces. Vertical grey bars are trenches excavated along the cross-section. (B) 2014 DEM of the WRPB with the location of the cross-sections indicated. (C) 2020 Orthomosaic of the WRPB. The extent of the orthomosaic is marked by a white dashed line and superimposed on a 2018 satellite image (Esri, 2018). (D) 2020 DSM of the WRPB. The extent of the DSM is denoted by a white dashed line and is superimposed on a 2018 satellite image (Esri, 2018).

trench in the middle of the transect, WR11, has a minor fining-upward trend of a 55 cm-thick F3 package topped by a finer 45 cm-thick F3 section (Fig. 2.9). Neither of these trenches have deposits that overlap with those of the 2014 point bar (Fig. 2.8; Fig. 2.9). The trench that does overlap with the 2014 profile, WR10, is at the end of the cross section. This trench begins with a fining-upwards trend where the 20 cm-thick F4 deposit at its base is overlain by 15 cm-thick F5 mud. Above the mud is a 10 cm-thick F3 deposit that coarsens upward to a 25 cm-thick F1 section. This coarser deposit is overlain by a thin 3 cm-thick bed of F5 that is followed by another 15 cm-thick F3 deposit (Fig. 2.8; Fig. 2.9).

The third cross section on WRPB, c-c', is the furthest downstream transect and has migrated approximately 80 m laterally since 2014. This has resulted in an estimated cross-sectional area of 345 m^2 of sediment deposited along this transect. The 2020 topographic profile does not contain any trenches that overlap with the 2014 topographic profile (Fig. 2.8). The 2014 profile has fewer and less exaggerated ridges and swales than the 2014 a-a' cross section. The 2020 topographic profile has two clear ridges with corresponding swales. The first trench that is closest to the channel, WR1, consisted of entirely F3 with no change to the grain size throughout (Fig. 2.10). The middle trench of the cross section was a series of three stacked trenches that comprise WR2. At the base of the lowest trench is a 23 cm-thick F3 deposit that is capped by a 2 cm-thick bed of F5. The mud layer is then succeeded a 55 cm-thick package of F3. The second trench in this series has two F3 packages that are bisected by a 2 cm-thick bed of F5. The upper-most trench in the section is entirely a F3 deposit, measuring 55 cm-thick. The mud throughout this sequence follows the slope of the point bar and is the same bed throughout the bottom two trenches (Fig. 2.10). The final trench along this cross section is WR12. At the base of this trench

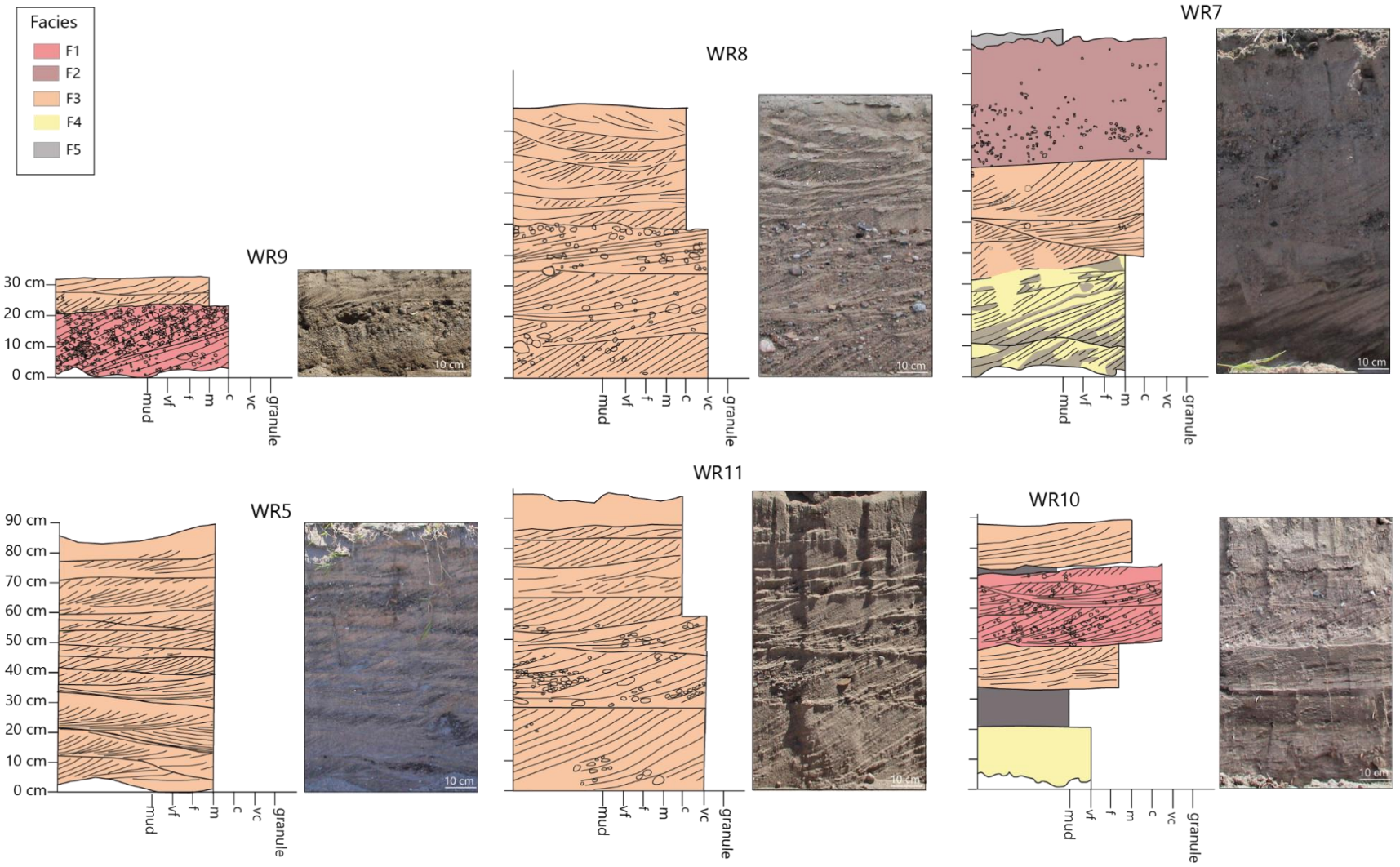

Fig 2.9. Sedimentary structures, facies, and trench photos of WR 9, WR 8, WR7, WR 5, WR 11, and WR 10. WR 9, WR 8, WR 5, and WR 11 all display the typical fining-upwards succession typical of point bar models. WR 7 coarsens-upward which is possibly due to extreme floods. WR 10 has both fining-upwards and coarsening-upwards successions.

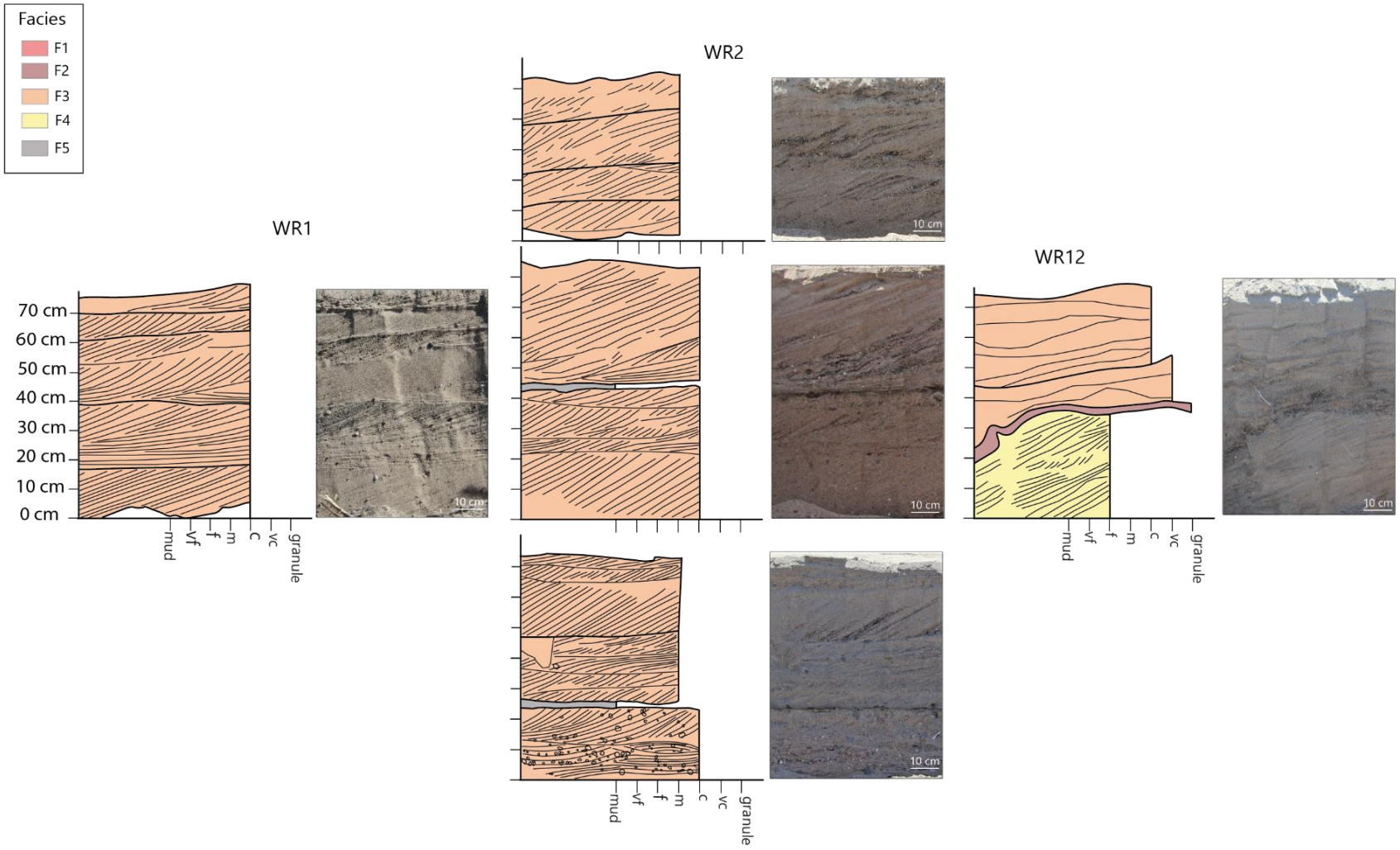

Fig 2.10. Sedimentary structure, facies, and trench photos of WR 1, WR 2, and WR12. WR 1 has no evident change in grain size; WR 2 has the typical fining-upward succession of a point bar. WR 12 coarsens-upward, potentially due to extreme floods.

is a 20 cm-thick F4 bed that is overlain by a 5 cm-thick F2 bed. The trench then has a 50 cm-thick F3 bed at its top (Fig. 2.10).

From when the LiDAR was collected in the fall of 2014 following the summer flood of 2014, to when the RPAS-SfM model was collected in the fall of 2020, extreme discharge occurred once in the spring of 2017. The two trenches that overlapped with the 2014 point bar had coarsening-upward sequences, including F1 and F2 gravel facies. The a-a' cross section is the axial zone of the point bar prior to the 2014 flood while the b-b' cross section is downstream of the former axial part of the bar. This supports the theory that over-bar flow extended the bar head flow configuration downstream of the point-bar axis resulting in gravels being deposited overtop of sand. WR12 also had a unique vertical succession where fine-grained strata is unconformably overlain by a thin gravel bed topped with a fining-upward very coarse-to-coarse sand interval. Based on the location of this cross section relative to the 2014 channel, it corresponds with deposition that occurred in 2015 when moderate flood stage was reached. Otherwise, the deposits on the point-bar either fine-upward or have a consistent grain-size throughout (e.g., WR1). Based on their locations along the transects, these sediments were not deposited during the moderate flood of 2015 like WR12 was, and most likely occurred during 2017 or 2019 when 21 m and 20 m of lateral accretion occurred, respectively. As extreme flood discharges were reached in 2017, this suggests that this flood did not alter the flow circulation in the same way the 2014 flood had.

In general, the FTPB model had greater overlap between 2014 and 2020 than the WRPB model over the same time period. This allowed for the estimation of the amount of sediment that was eroded along the cross sections in addition to the approximation of how much sediment had been deposited (Fig. 2.11).

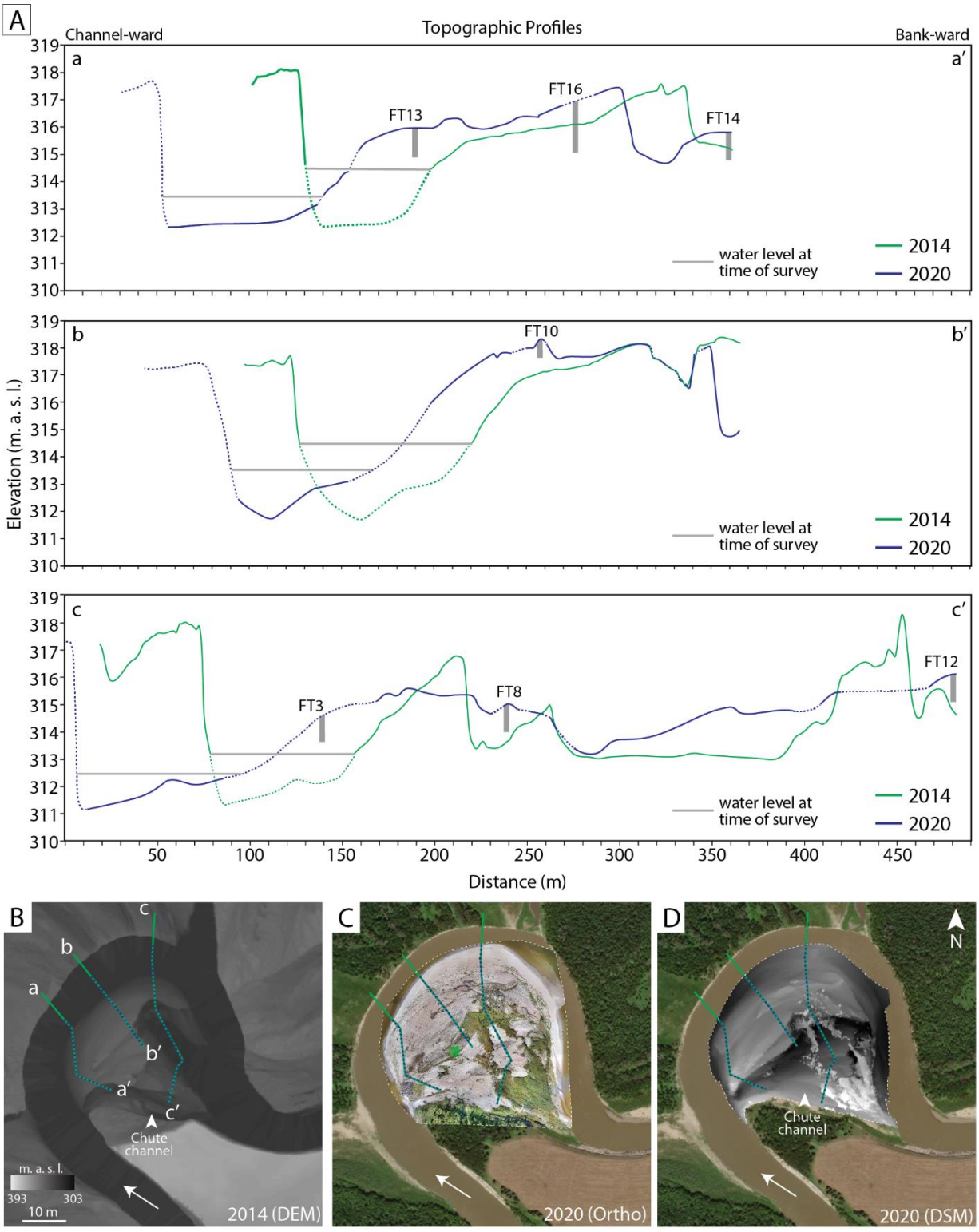

Fig 2.11. (A) Cross-sectional profiles of the FTPB. The 2014 profile (green solid line) is constructed froma DEM rendered from LiDAR captured fall 2014, post-2014 summer flood. The 2020 (blue solid line) profile is constructed from a DSM rendered from a RPAS-SfM model from summer 2020. Dashed lines indicate extrapolated surfaces. Vertical grey bars are trenches excavated along the cross-section. (B) 2014 DEM of the FTPB with the location of the cross-sections indicated. (C) 2020 Orthomosaic of the FTPB. The extent of the orthomosaic is marked by a white dashed line and superimposed on a 2018 satellite image (Esri, 2018). (D) 2020 DSM of the FTPB. The extent of the DSM is denoted by a white dashed line and is superimposed on a 2018 satellite image (Esri, 2018).

Cross section a-a’ is the furthest upstream of the three cross sections; it extends from a chute channel on the inner bank across the active channel to the cutbank. Along this transect the point bar has migrated laterally approximately 52 m with an estimated net area of 240 m^2 deposited and 80 m^2 eroded due to migration of the chute channel (Fig. 2.11). In 2014, this cross-sectional profile had a large ridge channel-ward followed by a deep chute channel. By 2020, the ridge had migrated significantly, with the chute channel eroding into the bank-ward side of the ridge. Additional ridge-and-swale topography formed since 2014 that does not have as large of a change in elevation. Both the 2014 and 2020 point bar slope steeply towards the channel. Three trenches were excavated along a-a’ to investigate recent deposition. FT13 was the closest to the active channel, and it was characterized by a 20 cm-thick F4 bed that was overlain by a 60 cm-thick F5 package. The lower 20 cm of the F5 bed contained vegetation and organics (Fig. 2.12). The other two trenches along the 2020 topographic profile intersect the contact with the 2014 point bar. FT16 consisted of a 60 cm-thick F1 bed at the base that was followed by a thin, 5 cm-thick F5 bed. The mud bed was overlain by a 55 cm-thick F2 bed that was also capped by a thicker, 25 cm-thick F5 bed (Fig. 2.12). Since 2014, the point bar has vertically accreted nearly 1 meter. The lower F5 bed is approximately 1 m below the present surface of the point bar and the top of bed is likely a boundary separating the 2014 deposits from the post-2014 deposits (Fig. 2.11; Fig. 2.12). The most bank-ward trench (FT14) along a-a’ is 1 m deep and characterized by a 50 cm-thick F2 bed at the base followed by a 50 cm-thick F1 bed from the middle to the top of the trench. At this location the point bar as accreted vertically approximately 50 cm. FT14 does not intersect the mud bed that was present in the FT16, however it is possible it was eroded by the chute channel as it expanded between 2014 and 2020, likely during overbank flow during the 2017 flood (Fig. 2.11; Fig. 2.12).

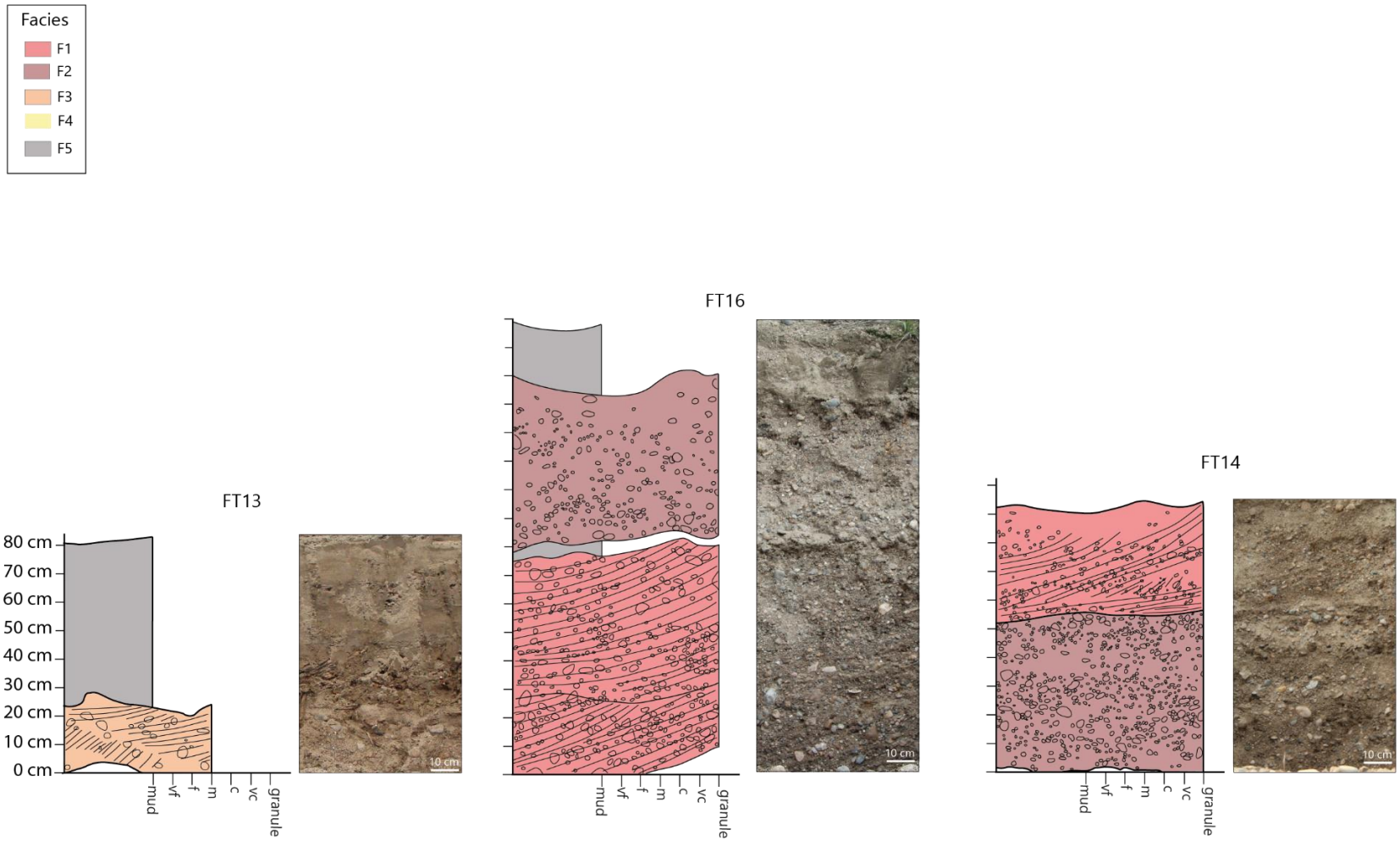

Fig 2.12. Sedimentary structure, facies and trench photos of FT 13, FT 16, FT 14. FT 13 is an F3 bed overlain by an F5 deposit, fining upwards. F16 consists of two gravel beds capped by mud. F14 has a massive gravel bed (F2) followed by a stratified gravel bed (F1).

The second cross section on the FTPB (b-b') is downstream of the bend apex of the point bar. The point bar has migrated laterally approximately 51 m at this position and has had an estimated net area of 250 m^2 of sediment deposited and 50 m^2 of sediment eroded (Fig. 2.11). Other than the lateral migration of the point bar, the 2020 profile of the bar and the 2014 profile are similar. A major ridge-and-swale from 2014 is the same in 2020, however, the most bank-ward ridge has been eroded significantly in 2020. A distinct scroll bar and chute channel remained unchanged. The only trench along this cross section, FT10, is 55 cm deep and consists entirely of F3 (Fig. 2.11; Fig. 2.12).

The third cross section on the FTPB (c-c') is near the bend apex of the point bar and is the longest cross section for this point bar. Along this cross section, the point bar has migrated laterally approximately 57 m, which has resulted in an estimated net area of 370 m^2 of sediment deposited and 70 m^2 of sediment eroded (Fig. 2.11). The profile of this bar has changed significantly between 2014 and 2020. The chute channel has aggraded several meters. The top of the ridges of two scroll bars have been eroded and their corresponding ridges have also vertically aggraded moderately. It is possible that the ridge bank-ward of the chute channel has not been eroded as much as shown in the profile as it was vegetated, limiting the scope of the DSM. Overall, the profile of the bar has become smoother and less exaggerated. FT3 is closest to the active channel and does not intersect deposits of pre-2014 point bar survey. FT3 is characterized by a 45 cm-thick F3 bed at the base that is in sharp contact with an overlying 5 cm-thick F5 bed. The F5 bed overlain by a 35 cm-thick F3 package at the top of the trench (Fig. 2.12). The middle trench along this cross section, FT8, is a 60 cm-thick F3 package that also does not intersect the 2014 point bar survey (Fig. 2.12). The most landward trench (FT12) is in a chute channel and is a 105 cm-thick F3 deposit with no variation in its strata (Fig. 2.12)

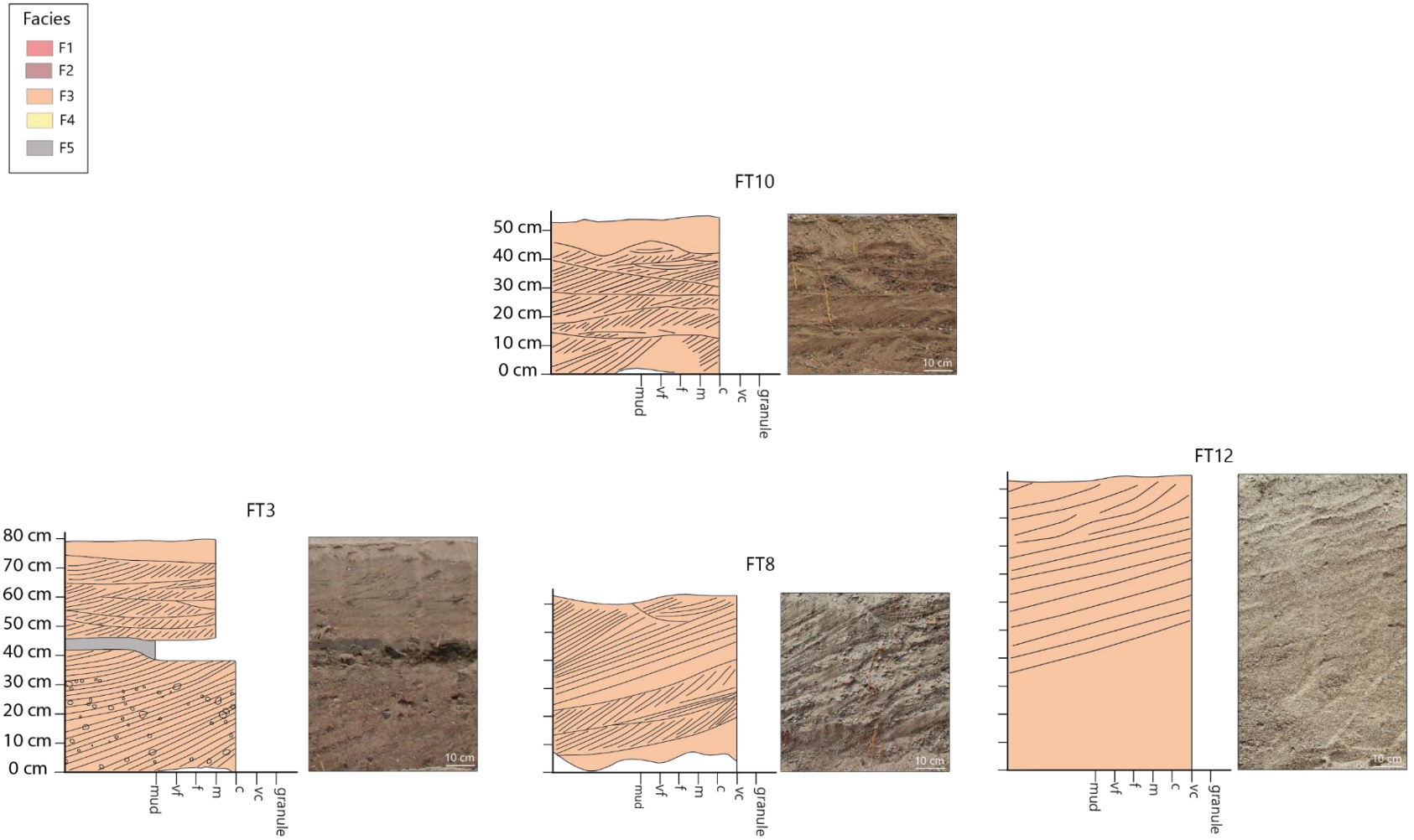

Fig 2.13. Sedimentary structures, facies and trench photos of FT 10, FT 3, FT 8, FT 12. FT10, FT 8, and FT12 are all F3 beds with no vertical succession. FT3 consists of two F3 beds bisected by a mud bed (F5).

The FTPB has not migrated as much as the WRPB since 2014, with migration occurring during moderate flood stage in 2015, extreme flood stage in 2017, and annual flow in 2019. None of the trenches had the upward-coarsening trend observed in the WRPB; however, they have several notable mud beds. FT13 and FT16 are both capped by thick beds of mud which is atypical of their position on the bar head. FT16 also has a second mud bed that bi-sects two gravel beds and, based on the depth of the bed, the top of the mud bed marks the end of the 2014 flood deposits. FT3 has a similar discontinuous mud bed and was, like FT13, deposited sometime after the 2014 flood. These two mud-packages and the mud bed capping FT16 may have been the result of the extreme discharge recorded in 2017 where flow breached the banks of the channel, as seen in satellite imagery (Fig. 2.14; Fig. 2.15). However, the high discharge was not sustained for an extended period. These thick mud deposits may have occurred from sediment settling from suspension in slack water after an extreme flow has waned (Church, 2006).

2.4.4. Channel Migration and Point Bar Evolution

Satellite imagery from 2010 to 2020 allows for the quantification of river channel migration and point bar evolution over time. In the past decade, WRPB has laterally migrated 360 m along the point bar axis, which has resulted in 0.14 km^2 of sediment deposited on the point bar and 0.15 km^2 eroded from the cutbank (Fig. 2.16; Fig. 2.17). The meander bend experienced a combination of expansion, translation, and rotation downstream during extreme flood events (e.g., Daniel, 1971). Over this period, the WRPB's path length has increased from 1.0 km to 1.4 km and its amplitude has increased from 0.13 km to 0.25 km, indicating expansion.

Fig 2.14. Satellite images of the Assiniboine River during annual flows (2010, 2013) and during extreme floods (2011, 2014). The channel during annual flow is superimposed on the river during extreme flooding to highlight the differences. The formation of a cut-off, floodplain inundation, over-bar flow, and the WRPB chute channel are indicated on the 2011 satellite image. The re-occupation of the abandoned channel and over-bar flow are indicated on the 2014 satellite image. Satellite images courtesy of Planet Labs.

Fig 2.15. Satellite images of the Assiniboine River during annual flow (2016) and during extreme flow (2017). The 2016 channel is superimposed on the 2017 image to highlight differences between annual flow and extreme discharge. Over-bar flows and abandoned channel re-occupation are highlighted. Satellite imagery courtesy of Planet Labs.

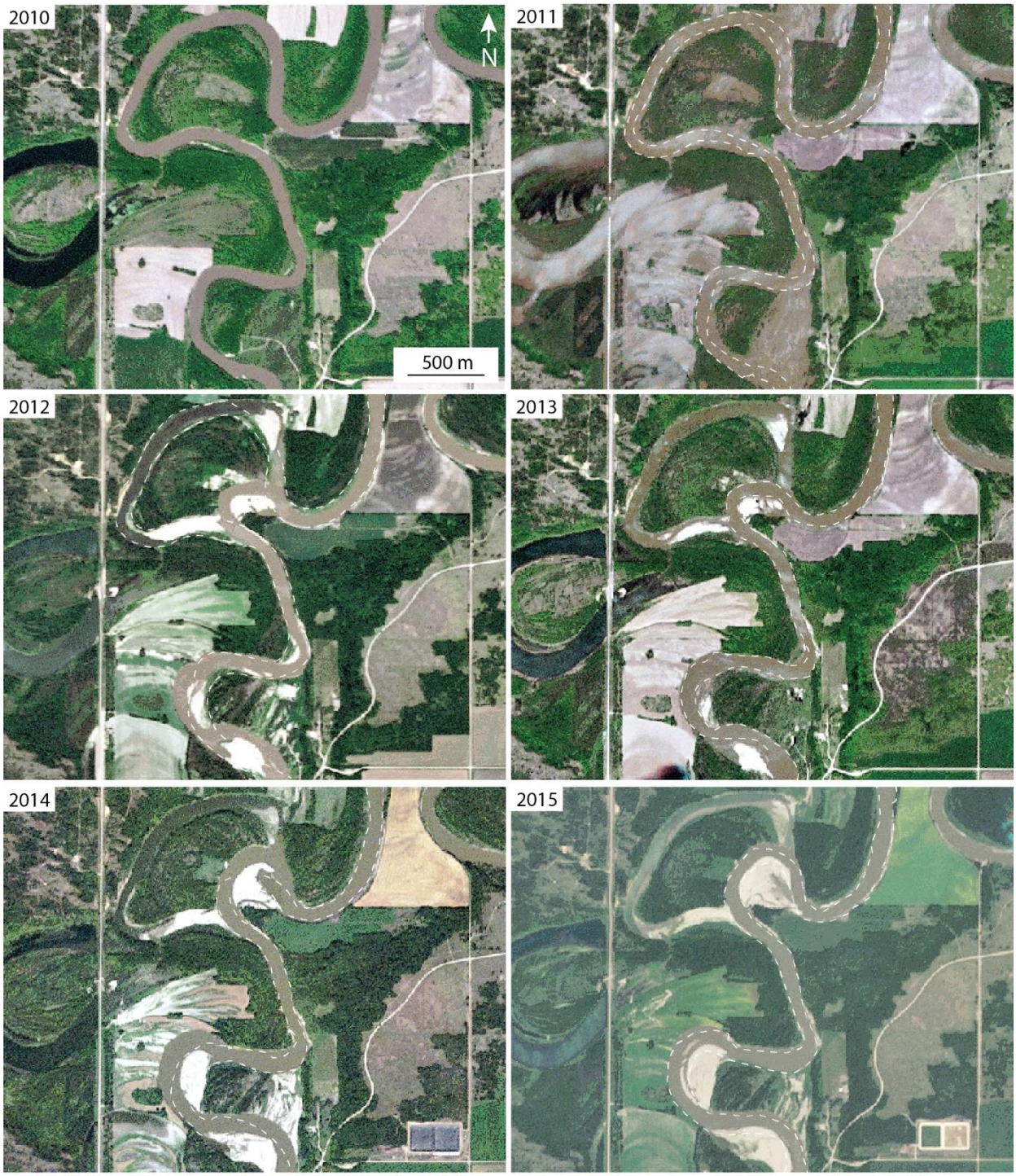

Fig 2.16. Geomorphic change occurring annually on the WRPB and FTPB from 2010 to 2015. The position of the channel the year prior is indicated in white dashed lines. Satellite images courtesy of Planet Labs.

Fig 2.17. Geomorphic change occurring annually on the WRPB and FTPB from 2016 to 2021. The position of the channel the year prior is indicated in white dashed lines. Satellite images courtesy of Planet Labs.

Sediment was eroded from the upstream portion of the point bar and deposition occurred downstream of the bend apex, resulting in translation. The ratio of sediment eroded from the WRPB upstream of the bend apex to the sediment deposited downstream of the bend apex, 1.22, is characteristic of rotation, in addition to the shift in bend axis typically associated with rotation (e.g., Ahmed et al., 2019). During the 2011 flood, the dominant mode of migration was translation and rotation. The channel eroded significantly into the upstream limb on the meander bend and sediment was deposited on the downstream limb of the meander, indicative of translation (e.g., Fig. 2.16). The axis of the point bar rotated in the downstream direction. The 2014 flood caused the point bar to expand and rotate; the pathlength and amplitude of the meander increased, and the point bar axis shifted downstream (e.g., Fig. 2.16). In 2017, the point bar once again migrated by expansion (e.g., Fig. 2.17).

Since the establishment of a new channel following the 2011 flood, the FTPB has mainly migrated through expansion and rotation. During the 2014 flood, the pathlength of the meander increased from 1.1 km to 1.5 km and the amplitude increased from 585 m to 685 m, indicative of expansion. The change in point bar axis downstream is also indicative of rotation occurring. In 2017, the meander bend experienced an increase in pathlength once again, migrating by expansion.

Most of the geomorphic change has occurred during extreme floods in 2011, 2014, and 2017 (Fig. 2.16; Fig. 2.17). For the WRPB, 291 m of 360 m of lateral migration occurred during extreme floods, or 80% of the total lateral migration. These events also resulted in the deposition of 0.092 km^2 of sediment and the erosion of 0.14 km^2 of sediment from the point bar. The erosion and deposition of sediment and the resulting meander migration has additionally altered the curvature of the bend. The initial WRPB had a radius of curvature of 344 m in 2010.

Following the 2011 extreme flood, the point bar bend radius of curvature decreased to 168 m in 2012. Since 2012, however, the radius of curvature of the bend has gradually increased to 205 m in 2014, 214 m in 2017, and 229 m in 2020. The FTPB has similarly had 80%, or 194 m, of its total lateral migration occur during these extreme floods. This migration is represented by 0.073 km^2 of sediment deposited on the point bar and the erosion of 0.10 km^2 of sediment from the cutbank this past decade. The point bar preceding the FTPB had a bend curvature with a radius of 314 m in 2010. Following the cut off which led to the formation of FTPB, the initial curvature of FTPB had a radius of 103 m. The radius of curvature gradually increased throughout the decade to 130 m in 2014, and 164 m in 2017 and 2020. Averaging the lateral migration of the two point bars over the last decade, the WRPB has migrated 36 m/yr and the FTPB has migrated 24 m/yr. However, it is clear from satellite imagery that this migration is not happening consistently every year and is occurring episodically during extreme floods. The rate of migration is influenced by several different factors such as bend curvature (Hickin & Nanson, 1975; Nanson & Hickin, 1983; Furbish, 1988; Sylvester et al., 2019), sediment supply (Constantine et al., 2014; Schwenk & Foufoula-Georgiou, 2016), and variations in bank erodibility (Sun et al., 1996; Guneralp and Rhoads, 2011; Bogoni et al., 2017).

Field measurements of the surficial sediment grain size were collected across the exposed point bar surface at low water (Fig. 2.18). Grain-size contour maps highlight two main trends: a decrease in grain size from upstream to downstream and an increase in grain size with age of the deposit (i.e. from the active channel inward on the bar). The upstream portion of the point bar consists of very coarse to coarse sand-sized grains, which fines towards the apex of the point bar that is dominantly medium-sand grains with some coarse sand, and finally the grain size fines further to the downstream portion of the point bar that consists of fine to very fine sand with

Fig 2.18. Map of surficial grain sizes on the WRPB. Overlain on a 2018 satellite image (Esri, 2018). Grain size decreases downstream and increases with distance from the channel.

mud. Downstream fining of grain-size is a well-established trend of point bars that has been observed in many studies (e.g., Jackson, 1981; Durkin et al., 2018). The grain-size trend is a direct result of cross-stream sediment transport and varying boundary shear stress that is inherent with meander bends as the zone of maximum shear stress crosses from the inside bank toward the pool at the bend apex (Dietrich & Smith, 1984).

While the grain-size trend around the bend is consistent with the literature, the grain-size distribution from channel to interior of the bar varies from what is typically expected. In the upstream portion of the point bar, the grain size transitions from coarse sand near the active channel to very coarse sand at the interior of the point bar. At the bend apex, the sediments similarly transition from medium sand to coarse sand with distance from the channel. Finally, at the downstream portion, the sand adjacent to the active channel is fine sand and the deposits at the interior of the bar are medium sand. Past studies on the grain-size trends of overbank deposits associated with extreme floods indicate that the median grain-size typically decreases with distance from the channel (Kesel, 1974; Walling et al., 1997). However, it is possible the results from this study are not consistent with the literature due to the scope of the surficial grain size survey. The formative studies typically cover the floodplain whereas this study only accounted for the active point bar. This is likely the result of coarser sediment being deposited on the bar top during extreme flood events when flow crosses over the bar during peak discharge (e.g., Ghinassi et al., 2018). This sediment is then not altered by lower-discharge events as these flows are confined to the channel, depositing finer sediment on the inner banks than what is present on the top of the bar.

2.5. Discussion

2.5.1. Point Bar Migration

The rate of migration of a meandering river is controlled by several factors, including bend curvature (i.e., Hickin & Nanson, 1975; Nanson & Hickin, 1983; Furbish, 1988; Sylvester et al., 2018), sediment discharge (i.e. Constantine et al., 2014; Schwenk & Foufoula-Georgiou, 2016), bank erodibility, and floodplain heterogeneity (i.e. Sun et al., 1996; Hudson and Kesel, 2000; Fryirs & Brieerly, 2010; Guneralp & Rhoads, 2011; Bogoni et al., 2017). Early studies on the relationship between bend curvature and migration rates suggested that migration rate is at its greatest when the radius of curvature is between two to three times the width of the river, with high-curvature bends migrating more slowly (Hickin & Nanson, 1975; Nanson & Hickin, 1983). However, recent research on the relationship between curvature and migration rate found that when the downstream shift of the migration rate relative to the local curvature is considered, a quasi-linear relationship between curvature and rate of migration emerges such that high curvature bends have high rates of migration (Sylvester et al., 2019). Another important migration rate factor that was highlighted by the study by Sylveset et al., (2019) was the importance of meander cutoffs in river migration, which in turn is related to sediment discharge as a factor that controls river migration. A study by Schwenk and Foufoula-Georgiou (2016) showed that cutoffs act as perturbations that nonlocally increase river migration upstream and downstream of the cutoff. These cutoffs inject downstream pulses of sediment excavated from the floodplain as the chute channel is formed (Fuller et al., 2003; Zinger et al., 2011; Schwenk and Foufoula-Georgiou, 2016). This is consistent with other research from the Amazon Basin that demonstrated rivers with higher sediment loads have high migration rates (Constantine et al., 2014). Finally, for partially confined meanders such as the Assiniboine River, the morphology and therefore migration is strongly controlled by antecedent controls of the river valley such as

the presence of bedrock or older, compacted sediment (i.e. the valley edge) and the previous deposits of the channel that make up the floodplain (Fryirs & Brierley, 2010).

The Assiniboine River in the chosen study area offers insight into the rate of migration of meandering rivers. The FTPB recently underwent a cut-off which served as a change in bend curvature and a pulse of sediment. Furthermore, while the WRPB did not experience a cut off, its channel was altered in 2016 through the addition of riprap upstream of the bend. In comparison with meanders on the Beatton River that have similar radius of bend curvature normalized to channel width as the Assiniboine River (i.e. in the range of 1 to 4), the migration rate of the studied bends on the Assiniboine River greatly exceeds that of the Beatton River by several orders of magnitude (Nanson and Hickin, 1983). The bend that migrated the fastest on the Beatton River had a reported 0.7 m/yr migration rate for a bend with a radius of curvature to channel width ratio of 2.65. In contrast, the WRPB and FTPB had migration rates of 36 m/yr and 24 m/yr, respectively. The WRPB experienced the greatest lateral migration and the fastest migration rates during the 2011 and 2014 extreme floods; the FTPB similarly had the most lateral migration and fastest migration during the 2014 flood. During these extreme floods, flow over the bar decreased these bend's radius of curvature, resulting in temporarily higher curvature bends (Fig. 2.14). As the radius of curvature increased over time, the point bars experienced less lateral migration and thus, lower rates of migration. The difference in lateral migration during each flood is not solely the product of bend curvature as the discharges during the 2014 and 2017 floods were lower than in 2011 but all three flow events had over-bar flow (Fig. 2.15).

While direct measurements of sediment discharge do not exist for the Assiniboine River, the cut off and chute channel that occurred at the FTPB and WRPB, respectively, injected pulses of sediment excavated from the floodplain which may have increased migration rates similarly to

increased rates documented by Schwenk and Foufoula-Georgiou (2016). The rates of migration recorded for the two point bars in this study, 36 m/yr and 24 m/yr, are more similar to migration rates documents in the Amazonian basin than the migration rates documented on other Canadian rivers.. From a study by Constantine et al., (2014), the average rate of migration for the 20 studied reaches of the Amazon was 8.873 m/yr with the highest reported rate being 21.615 m/yr from the Mamoré reach and the lowest reported rate from the Xingu reach at 1.311 m/yr.

In the study area the river is first degree confined and proximal to the valley wall located in the south-east. The two point bars of interest are migrating away from this boundary, which allows them to migrate relatively unimpeded. Furthermore, the FTPB is in the process of reoccupying the former meander loop, growing in the same direction and location as the previous point bar. This is likely due to the relatively uncompacted sediment of the previous point bar, allowing for easy erosion of the cutbank (Perruca et al., 2007; Camporeale et al., 2008). Based on field observation that is supported by satellite imagery, the abandoned meander has not been entirely filled with erosion-resistant sediment and is re-occupied during high discharge flows (Fig. 2.17; Fig. 2.18). While the WRPB and FTPB have migrated laterally quite significantly over the past decade, it is in stark contrast to the point bar in between them and the next point bar downstream of FTPB that have hardly migrated during this ten year period of observation. Looking at the DEM of the 2014 LiDAR, it is evident that the two point bars that were investigated in this study are migrating towards the more easily eroded former channels in the floodplain, whereas the two point bars that have not migrated are limited by the valley wall and a terrace (Fig. 2.1). Further proof of the inability for the Assiniboine River to erode into the terrace is that when the 2011 cutoff occurred, it did not cross the terrace and the new point bar began at the edge of the terrace (Fig. 2.11(b)).

Based on the results of this study, the increased rate of migration in the study area is the result of floodplain heterogeneity, such as the more easily erodible former channels, and extreme floods which alter bend curvature and inject pulses of sediment.

2.5.2. Sedimentology

Based on the classic model of point-bar facies, the fining-upwards grain-size trend is a key criterion for identifying point bars in the sedimentary record (Allen, 1965a; McGowen & Garner, 1970; Bluck, 1971). However, recent studies have revealed exceptions to this model that demonstrate a coarsening-upwards trend (e.g., Costa, 1974; Fisk, 1974; Knox, 1987; Ghinassi et al., 2018; Hagstrom et al., 2018). Recent studies by Ghinassi et al., (2018) and Hagstrom et al., (2018) have integrated remote sensing and field investigations to improve our understanding of point bar morphodynamics and sediment distribution. A study by Ghinassi et al. (2018) documented morphological evidence of flow at flood stage crossing over the point bar, shifting the zone of maximum outer bank erosion downstream. This was further supported by sedimentological evidence of an overall coarsening-upward grain size trend and bar armoring. In contrast, the annual deposits were consistent with the classic model of fining-upward grain-size trend (Ghinassi et al., 2018). Hagstrom et al. (2018) concluded that no single grain-size nor sedimentary structure is indicative of an extreme flood; however, in the floodplain, flood deposits were coarser than normal floodplain deposits.

The deposits exposed on the Assiniboine River have some evidence in support of a coarsening-upward trend associated with extreme floods. Deposits on the bar head are known to be coarse-grained, with flow directed outwards from the bar towards the point of maximum erosion on the cutbank (Bluck, 1971; Jackson, 1976). When extreme discharges occur, flow

breaches the banks of the channel and flow over the point bar. This alters the dynamics of the flow, widening the flow area and decreasing the curvature. Flow is directed orthogonal to the point bar, shifting the bar head morphodynamics downstream past the axis of the point bar (Kasvi et al., 2017; Ghinassi et al., 2018). This causes coarser sediments to be deposited overtop of the finer deposits typical of the axial zone of the point bar. The change in flow direction also shifts the point of maximum erosion downstream, past the point bar axis (Ghinassi et al., 2018). These processes are supported by the 2014 flood deposits exposed on the WRPB, the morphological change of the WRPB in 2011 and 2014, and the morphological change of the FTPB in 2014.

Satellite images of the study area during peak flow in 2011 and 2014 show water flowing over the point bars (Fig. 2.14). Satellite images also indicate that maximum erosion occurred downstream of the point bar axis, supporting flow being directed orthogonal to the point bar. This resulted in the rotation of the point bars as they migrated, where the axis of the two point bars shifted downstream. Furthermore, WR7, WR10, and WR12 trenches were comprised of coarsening-upward sequences, which were deposited either along the point bar axis or downstream of it, indicating the spread of bar-head hydrodynamics over the point bar axis. However, a coarsening-upward sequence was absent from the FTPB trenches. On the FTPB, the 2014 extreme flood was recorded by a mud bed bisecting two gravel beds. This package of mud was tied to the 2014 flood using the depth of the deposit and the two point bar profiles (Fig. 2.11). While extreme floods may sometimes result in a deviation from the classical point-bar model, as was the case with Ghinassi et al. (2018) and the WRPB, further investigation is required to understand the full complexity of the flow dynamics that vary from meander bend to meander bend.

While there was some deviation in the sedimentary deposits, the greatest difference for these meander bends between extreme floods and annual flows is the rate of migration. As previously discussed, the rate of migration for these meander bends this past decade was extremely high with 80% of migration occurring during extreme floods (i.e., 2011, 2014) or extreme discharge events (i.e., 2017). As migration occurs, sediment is deposited as the meander erodes into the cutbank. Thus, with increased rates of migration there is an increased rate of sediment deposition. Therefore, the sediments may not differ from the typical point bar facies, but there are more of them, and they have been deposited much faster than annual flow deposits. This is different from studies by Gomez et al. (1995) and Heitmuller et al. (2017) on the lack of sedimentation on the Mississippi River following the 1993 and 2011 floods, respectively. This highlights a need to further investigate the rate of migration and associated sedimentation during extreme floods on meandering rivers.

2.6. Conclusion

Extreme floods have a significant morphological and sedimentological impact on the Assiniboine River. In the study area, the two point bars that are not limited by the valley wall migrate laterally at a much faster rate, particularly during extreme flows. During extremely high discharge events, flow expands overtop of the point bar, shifting the point of maximum erosion downstream and causing rotation of the point bar as it migrates laterally. As the point bars rapidly migrate laterally, a significant amount of sediment is deposited. In some instances, such as the WRPB, the deposits of extreme floods vary from that of annual flows with a coarsening-upwards vertical succession. However, on the point bar that was newly formed during the 2011

flood, the point bar sedimentology adhered to the classical fining-upwards model with a discontinuous mud bed associated with the 2014 flood.

Fully understanding how flows of various discharges effect sedimentary deposits and their distribution is essential for reconstructing the sedimentary record. This contributes to a continued refinement of sedimentary facies models that are used for hydrocarbon reservoirs and aquifer management (McKie et al., 2010; Colombera et al., 2017). More locally, understanding the flood deposits on the Assiniboine River provides a means to extend the flood hydrograph past the human record. This will improve flood prediction models, providing insight into the likelihood of a flood of a given magnitude and the geomorphic change that is likely to occur as a result.

2.7. References

Allen, J. R. (1965a). A review of the origin and characteristics of recent alluvial sediments. *Sedimentology*, *5*(2), 89-191.

Allen, J. R. L. (1965b). Sedimentation to the lee of small underwater sand waves: an experimental study. *The Journal of Geology*, *73*(1), 95-116.

Allen, J. R. L. (1970). Studies in fluviatile sedimentation: a comparison of fining-upwards cyclothems, with special reference to coarse-member composition and interpretation. *Journal of Sedimentary Research, 40*(1).

Allen, J.R.L. (1982) Sedimentary Structures. Their Character and Physical Basis. Volume I. Elsevier, 1–663 pp.

Ahmari, H., Blais, E-L. and Greshuk, J. (2016). The 2014 flood event in the Assiniboine River Basin: Causes, assessment, and damages. *Canadian Water Resources Journal*, *41*(1-2), 85-93.

Ahmed, J., Constantine, J. A., & Dunne, T. (2019). The role of sediment supply in the adjustment of channel sinuosity across the Amazon Basin. *Geology*, *47*(9), 807–810.

Andrle, R. (1996). Measuring channel planform of meandering rivers. Physical Geography, 17(3), 270-281.

Arnell, N. W., & Gosling, S. N. (2016). The impacts of climate change on river flood risk at the global scale. *Climatic Change*, *134*(3), 387-401.

Bathurst, J. C., Thorne, C. R., & Hey, R. D. (1977). Direct measurements of secondary currents in river bends. *Nature*, *269*(5628), 504-506.

Bridge, J. S., & Jarvis, J. (1976). Flow and sedimentary processes in the meandering river South Esk, Glen Clova, Scotland. *Earth surface processes*, *1*(4), 303-336.

Bridge, J. S., Alexander, J. A. N., Collier, R. E. L., Gawthorpe, R. L., & Jarvis, J. (1995). Ground-penetrating radar and coring used to study the large-scale structure of point-bar deposits in three dimensions. *Sedimentology*, *42*(6), 839-852.

Brimelow, J., Szeto, K., Bonsal, B., Hanesiak, J., Kochtubajda, B., Evans, F., & Stewart, R. (2015). Hydroclimatic aspects of the 2011 Assiniboine River Basin flood. *Journal of Hydrometeorology*, *16*(3), 1250-1272.

Blais, E-L., Greshuk, J. and Stadnyk, T. (2016a). The 2011 flood event in the Assiniboine River Basin: Causes, assessment, and damages. *Canadian Water Resources Journal, 41*(1-2), 74-84.

Blais, E-L., Clark, S., Dow, K., Rannie, B., Stadnyk, T. and Wazney, L. (2016b). Background to flood control measures in the Red and Assiniboine River Basins. *Canadian Water Resources Journal, 41*(1-2), 31-44.

Bluck, B. J. (1971). Sedimentation in the meandering River Endrick. Scottish Journal of *Geology, 7*(2), 93-138.

Bogoni, M., Putti, M., & Lanzoni, S. (2017). Modeling meander morphodynamics over self-formed heterogeneous floodplains. *Water Resources Research, 53*(6), 5137-5157.

Boyd, M. (2007). Early postglacial history of the southeastern Assiniboine Delta, glacial Lake Agassiz basin. *Journal of Paleolimnology*, *37*(3), 313-329.

Camporeale, C., Perucca, E., & Ridolfi, L. (2008). Significance of cutoff in meandering river dynamics. *Journal of Geophysical Research: Earth Surface*, *113*(F1).

Carling, P. A. (1996). Morphology, sedimentology and palaeohydraulic significance of large gravel dunes, Altai Mountains, Siberia. *Sedimentology, 43*(4), 647-664.

Constantine, J. A., Dunne, T., Ahmed, J., Legleiter, C., & Lazarus, E. D. (2014). Sediment supply as a driver of river meandering and floodplain evolution in the Amazon Basin. *Nature Geoscience, 7*(12), 899-903.

Church, M. (2006). Bed material transport and the morphology of alluvial river channels. *Annual Review of Earth and Planetary Science, 34*, 325-354.

Costa, J. E. (1974a). Response and recovery of a Piedmont watershed from tropical storm Agnes, June 1972. *Water Resources Research, 10*(1), 106-112.

Costa, J. E. (1974b). Stratigraphic, morphologic, and pedologic evidence of large floods in humid environments. *Geology, 2*(6), 301-303.

Daniel, J. F. (1971). *Channel movement of meandering Indiana streams* (No. 732). US Government Printing Office.

Dietrich, W. E., Smith, J. D., & Dunne, T. (1979). Flow and sediment transport in a sand bedded meander. *The Journal of Geology, 87*(3), 305-315.

Dietrich, W. E., & Smith, J. D. (1983). Influence of the point bar on flow through curved channels. *Water Resources Research, 19*(5), 1173-1192.

Dietrich, W. E., & Smith, J. D. (1984). Bed load transport in a river meander. *Water Resources Research*, *20*(10), 1355-1380.

Dinehart, R. L. (1992). Evolution of coarse gravel bed forms: Field measurements at flood stage. *Water Resources Research*, *28*(10), 2667-2689.

Durkin, P. R., Hubbard, S. M., Smith, D. G., & Leckie, D. A. (2018). Predicting heterogeneity in meandering fluvial and tidal-fluvial deposits: The point bar to counter point bar transition. *Fluvial Meanders and Their Sedimentary Products in the Rock Record*, 231-249.

Esri. (July 17, 2018). World Topographic Map. http://www.arcgis.com/home/item.html?id=30e5fe3149c34df1ba922e6f5bbf808f (Accessed October 29, 2022).

Fenton, M. M. (1970). The Pleistocene stratigraphy and surficial geology of the Assiniboine River to Lake Manitoba area, Manitoba. M. Sc Thesis, University of Manitoba, Winnipeg, Manitoba.

Fisk, L. H. (1974). Inverse grading as stratigraphic evidence of large floods: Comment. *Geology*, *2*(12), 613-614.

Fryirs, K., & Brierley, G. J. (2010). Antecedent controls on river character and behaviour in partly confined valley settings: Upper Hunter catchment, NSW, Australia. *Geomorphology*, *117*(1-2), 106-120.

Furbish, D. J. (1988). River-bend curvature and migration: How are they related?. *Geology*, *16*(8), 752-755.

Gardner, J. S. (1977). Some geomorphic effects of a catastrophic flood on the Grand River, Ontario. *Canadian Journal of Earth Sciences*, *14*(10), 2294-2300.

Ghinassi, M., Moody, J., & Martin, D. (2018). Influence of extreme and annual floods on point-bar sedimentation: Inferences from Powder River, Montana, USA. *GSA Bulletin*, *131*(1-2), 71-83.

Gomez, B., Mertes, L. A., Phillips, J. D., Magilligan, F. J., & James, L. A. (1995). Sediment characteristics of an extreme flood: 1993 upper Mississippi River valley. *Geology*, *23*(11), 963-966.

Google Earth 7.3. (April 27, 2011). Spruce Woods Provincial Park. 40°40’32.24” N, 99°15’47.80” W, 4.94 km. http://www.google.com/earth/index.html (Accessed October 29, 2022).

Google Earth 7.3. (August 24, 2013). Spruce Woods Provincial Park. 40°40’32.24” N, 99°15’47.80” W, 4.94 km. http://www.google.com/earth/index.html (Accessed October 29, 2022).

Google Earth 7.3. (June 26, 2017). Spruce Woods Provincial Park. 40°40’32.24” N, 99°15’47.80” W, 4.94 km. http://www.google.com/earth/index.html (Accessed October 29, 2022).

Government of Manitoba [GOM]. (2013). 2011 Flood: Technical Review of Lake Manitoba, Lake St. Martin and Assiniboine River Water Levels. Retrieved April 2021 from: https://content.gov.mb.ca/mit/wm/assiniboine_lakemb_lsm_report_nov2013.pdf

Government of Manitoba [GOM]. (2021). Water Information and Flood Conditions; Forecasts/Reports. Retrieved Nov 2021 from: https://gov.mb.ca/mit/floodinfo/

Guan, M., Carrivick, J. L., Wright, N. G., Sleigh, P. A., & Staines, K. E. (2016). Quantifying the combined effects of multiple extreme floods on river channel geometry and on flood hazards. *Journal of Hydrology*, *538*, 256-268.

Güneralp, İ., & Rhoads, B. L. (2011). Influence of floodplain erosional heterogeneity on planform complexity of meandering rivers. *Geophysical Research Letters*, *38*(14).

Gupta, A. (1983). High-magnitude floods and stream channel response. *Modern and ancient fluvial systems*, 219-227.

Hagstrom, C. A., Leckie, D. A., & Smith, M. G. (2018). Point bar sedimentation and erosion produced by an extreme flood in a sand and gravel-bed meandering river. *Sedimentary geology*, *377*, 1-16.

Heitmuller, F. T., Hudson, P. F., & Kesel, R. H. (2017). Overbank sedimentation from the historic AD 2011 flood along the Lower Mississippi River, USA. *Geology*, *45*(2), 107-110.

Hickin, E. J., & Nanson, G. C. (1975). The character of channel migration on the Beatton River, northeast British Columbia, Canada. *Geological Society of America Bulletin*, *86*(4), 487-494.

Hickin, E. J., & Nanson, G. C. (1984). Lateral migration rates of river bends. *Journal of Hydraulic Engineering*, *110*(11), 1557-1567.

Hickin, E. J., & Sichingabula, H. M. (1988). The geomorphic impact of the catastrophic October 1984 flood on the planform of Squamish River, southwestern British Columbia. *Canadian Journal of Earth Sciences*, *25*(7), 1078-1087.

Hooke, R. L. B. (1975). Distribution of sediment transport and shear stress in a meander bend. *The Journal of geology*, *83*(5), 543-565.

Hudson, P. F., & Kesel, R. H. (2000) Channel migration and meander-bend curvature in the lower Mississippi River prior to major human modification. *Geology, 28* (6): 531–534.

Jablonski, B. V., & Dalrymple, R. W. (2016). Recognition of strong seasonality and climatic cyclicity in an ancient, fluvially dominated, tidally influenced point bar: Middle McMurray Formation, Lower Steepbank River, north-eastern Alberta, Canada. *Sedimentology*, *63*(3), 552-585.

Jackson, R. G. (1976). Depositional model of point bars in the lower Wabash River. *Journal of Sedimentary Research*, *46*(3), 579-594.

Kasvi, E., Vaaja, M., Alho, P., Hyyppä, H., Hyyppä, J., Kaartinen, H., & Kukko, A. (2013). Morphological changes on meander point bars associated with flow structure at different discharges. *Earth Surface Processes and Landforms*, *38*(6), 577-590.

Kasvi, E., Laamanen, L., Lotsari, E., & Alho, P. (2017). Flow patterns and morphological changes in a sandy meander bend during a flood—Spatially and temporally intensive ADCP measurement approach. *Water*, *9*(2), 106.

Kesel, R. H., Dunne, K. C., McDonald, R. C., Allison, K. R., & Spicer, B. E. (1974). Lateral erosion and overbank deposition on the Mississippi River in Louisiana caused by 1973 flooding. *Geology*, *2*(9), 461-464.

Kehew, A. E., & Teller, J. T. (1994). History of late glacial runoff along the southwestern margin of the Laurentide ice sheet. *Quaternary Science Reviews*, *13*(9-10), 859-877.

Klassen, R. W. (1972). Wisconsin events and the Assiniboine and Qu'Appelle valleys of Manitoba and Saskatchewan. *Canadian Journal of Earth Sciences*, *9*(5), 544-560.

Knox, J. C. (1987). Stratigraphic evidence of large floods in the upper Mississippi Valley. *In Catastrophic flooding (pp. 155-180)*. Routledge.

Kundzewicz, Z. W., Pińskwar, I., & Brakenridge, G. R. (2013) Large floods in Europe, 1985–2009, *Hydrological Sciences Journal*, *58*(1), 1-7.

Lamb, M. P., de Leeuw, J., Fischer, W. W., Moodie, A. J., Venditti, J. G., Nittrouer, J. A., Haught, D. & Parker, G. (2020). Mud in rivers transported as flocculated and suspended bed material. *Nature Geoscience*, *13*(8), 566-570.

Leeder, M. R., & Bridges, P. H. (1975). Flow separation in meander bends. *Nature, 253*(5490), 338-339.

Leeder, M. R. (2011). Tectonic sedimentology: sediment systems deciphering global to local tectonics. *Sedimentology, 58*(1), 2-56.

Leopold, L.B., and Wolman, M.G. (1960) River meanders: Geological Society of America Bulletin, v. 71, p. 769–793

Lewin, J., & Brindle, B. J. (1977). Confined meanders. *River channel changes*, 221-233.

Magilligan, F. J., Phillips, J. D., James, L. A., & Gomez, B. (1998). Geomorphic and sedimentological controls on the effectiveness of an extreme flood. *The Journal of geology, 106*(1), 87-96.

McGowen, J. H., & Garner, L. E. (1970). Physiographic features and stratification types of coarse-grained point bars: modern and ancient examples 1. *Sedimentology, 14*(1-2), 77-111.

Miall, A. D. (1985). Architectural-element analysis: a new method of facies analysis applied to fluvial deposits. *Earth-Science Reviews, 22*(4), 261-308.

Miall, A. D. (2010). Alluvial Deposits. In N.P. James & R. W. Dalrymple (Eds.), *Facies Model 4* (pp. 105-137). Geological Association of Canada.

Miller, A. J. (1990). Flood hydrology and geomorphic effectiveness in the central Appalachians. *Earth Surface Processes and Landforms*, *15*(2), 119-134.

Nanson, G. C. (1980). Point bar and floodplain formation of the meandering Beatton River, northeastern British Columbia, Canada. *Sedimentology*, *27*(1), 3-29.

Nanson, G. C., & Hickin, E. J. (1983). Channel migration and incision on the Beatton River. *Journal of Hydraulic Engineering*, *109*(3), 327-337.

Nanson, G. C. (1986). Episodes of vertical accretion and catastrophic stripping: a model of disequilibrium flood-plain development. *Geological Society of America Bulletin*, *97*(12), 1467-1475.

Nicoll, T. J., & Hickin, E. J. (2010). Planform geometry and channel migration of confined meandering rivers on the Canadian prairies. *Geomorphology*, *116*(1-2), 37-47.

Perucca, E., Camporeale, C., & Ridolfi, L. (2007). Significance of the riparian vegetation dynamics on meandering river morphodynamics. *Water Resources Research*, *43*(3).

Planet Team (2017). Planet Application Program Interface: In Space for Life on Earth. San Francisco, CA. https://api.planet.com.

Rannie, W. F., Thorleifson, L. H., & Teller, J. T. (1989). Holocene evolution of the Assiniboine River paleochannels and Portage la Prairie alluvial fan. *Canadian Journal of Earth Sciences*, *26*(9), 1834-1841.

Reesink, A. J. H., Van den Berg, J. H., Parsons, D. R., Amsler, M. L., Best, J. L., Hardy, R. J., Orefo, O. & Szupiany, R. N. (2015). Extremes in dune preservation: Controls on the completeness of fluvial deposits. *Earth-Science Reviews*, *150*, 652-665.

Sambrook Smith, G. H., Best, J. L., Ashworth, P. J., Lane, S. N., Parker, N. O., Lunt, I. A., Thomas, R. E. & Simpson, C. J. (2010). Can we distinguish flood frequency and magnitude in the sedimentological record of rivers?. *Geology*, *38*(7), 579-582.

Schwenk, J., & Foufoula-Georgiou, E. (2016). Meander cutoffs nonlocally accelerate upstream and downstream migration and channel widening. *Geophysical Research Letters*, *43*(24), 12-437.

Stewart, J. H., & LaMarche, V. C. (1967). *Erosion and deposition produced by the flood of December 1964 on Coffee Creek, Trinity County, California*. US Government Printing Office.

Smith, N. D. (1972). Some sedimentological aspects of planar cross-stratification in a sandy braided river. *Journal of Sedimentary Research*, *42*(3), 624-634.

Sylvester, Z., Durkin, P., & Covault, J. A. (2019). High curvatures drive river meandering. *Geology*, *47*(3), 263-266.

Sun, T., Meakin, P., Jøssang, T., & Schwarz, K. (1996). A simulation model for meandering rivers. *Water resources research*, *32*(9), 2937-2954.

Tierney, J. E., Poulsen, C. J., Montañez, I. P., Bhattacharya, T., Feng, R., Ford, H. L., Honisch, B., Inglis, G. N., Petersen, S. V., Sagoo, N., Tabor, C. R., Thirumalai, K., Zhu, J., Burls, N. J., Godderis, Y., Foster, G. L., Huber, B. T., Ivany, L. C., Turner, S. K., Lunt, D. J., McElwain, J. C., Mills, B. J. W., Otto-Bliesner, B. L., Ridgewell, A. & Zhang, Y. G. (2020). Past climates inform our future. *Science*, *370*(6517).

Tu, T., Carr, K. J., Ercan, A., Trinh, T., Kavvas, M. L., & Nosacka, J. (2017). Assessment of the effects of multiple extreme floods on flow and transport processes under competing flood protection and environmental management strategies. *Science of the Total Environment*, 607, 613-622.

Turner, D., Lucieer, A., & Watson, C. (2012). An automated technique for generating georectified mosaics from ultra-high resolution unmanned aerial vehicle (UAV) imagery, based on structure from motion (SfM) point clouds. *Remote sensing*, *4*(5), 1392-1410.

Walling, D. E., Owens, P. N., & Leeks, G. J. L. (1997). The characteristics of overbank deposits associated with a major flood event in the catchment of the River Ouse, Yorkshire, UK. *Catena*, *31*(1-2), 53-75.

Wolman, M. G., & Eiler, J. P. (1958). Reconnaissance study of erosion and deposition produced by the flood of August 1955 in Connecticut. *EOS, Transactions American Geophysical Union*, *39*(1), 1-14.

Wolman, M. G., & Gerson, R. (1978). Relative scales of time and effectiveness of climate in watershed geomorphology. *Earth surface processes*, *3*(2), 189-208.

Wolman, M. G., & Miller, J. P. (1960). Magnitude and frequency of forces in geomorphic processes. *The Journal of Geology*, *68*(1), 54-74.

Wolowich, E. A. (1985). *Sediment dynamics and flow analysis of the Assiniboine River* (Master's thesis).

Wysocki, N., & Hajek, E. (2021). Mud in sandy riverbed deposits as a proxy for ancient fine-sediment supply. *Geology*.

Table 2.1. Facies

Facies	Grain size/sorting	Sedimentary Structures	Colour	Bedding	Upper/lower contacts	Process Interpretation	Depositional Setting
F1: Cross-stratified coarse sand	cL to vcU, moderately to poorly sorted	Tabular cross-stratification, graded foresets, pebble to cobble size clasts at base of the bed, pebble to cobble size clasts	Light to medium yellow-y brown, dark grey	Bed thickness =30 cm to 60 cm Foreset thickness = 10 to 40cm	Sharp base and top	High energy unidirectional flow, fluctuating discharge	Upper to middle point bar
F2: Massive coarse sand	cL to vcL, poorly sorted	Pebble to cobble size clasts	Light to medium yellow-y brown	Bed thickness = 40 to 60 cm	Sharp base, sharp top	Rapid deposition from suspension in high energy flows	Upper point bar
F3: Cross-stratified medium sand	mL to mU, moderately to poorly sorted	Tabular cross-stratification, graded foresets, coarse grain clasts at base of the bed, granule to pebble size clasts	Light to medium yellow-y brown, dark grey	Bed thickness = 15 to 50 cm Foreset thickness = 3 to 10 cm	Sharp base and top	Moderate energy unidirectional flow, fluctuating discharge	Throughout point bar and lower counter point bar
F4: Cross-stratified fine sand	fL to fU, well to moderately sorted	Tabular cross-stratification, tabular cross-laminations, mud drapes on foresets, coarser grained clasts at base of the bed,	Light to medium yellow-y brown, dark brown mud drapes	Bed thickness = 10 cm to 40 cm Foreset thickness = 1 to 5 cm	Sharp base, shar and gradational top	Low energy unidirectional flow, fluctuating discharge	Counter point bar

		granule size clasts					
L5: Mud	Silt and clay, organic detritus	Organic debris	Dark grey to dark brown	Bed thickness = 1 cm to 40 cm	Sharp base, sharp and gradational top	Settling from suspension	Overbank

Table 2. Total Geomorphic Change

	Winter Rec Point Bar (WRPB)	Fallen Tree Point Bar (FTPB)
2010 Wavelength	1.0 km	2.6 km
2020 Wavelength	1.4 km	1.2 km
2010 Amplitude	0.13 km	0.45 km
2020 Amplitude	0.25 km	0.20 km
2010 Sinuosity	1.7	9.0
2020 Sinuosity	4.2	3.2
Lateral Migration	360 m	243 m
Rate of Migration	36 m/yr	24 m/yr
Area of Deposition	0.14 km^2	0.10 km^2
Area of Erosion	0.15 km^2	0.12 km^2

Table 3. Annual Geomorphic Change

	Lateral Migration (m)		Area Deposited (m^2)		Area Eroded (m^2)	
	WRPB	FTPB	WRPB	FTPB	WRPB	FTPB
2011	0	0	0	0	0	0
2012	150	*	58,000	*	57,000	*
2013	0	0	0	0	0	0
2014	120	160	25,000	57,000	64,000	75,000
2015	52	36	28,000	15,000	12,000	18,000
2016	0	0	0	0	0	0
2017	21	34	9,800	16,000	20,000	29,000
2018	0	0	0	0	0	0
2019	20	13	22,000	15,000	0	0
2020	0	0	0	0	0	0
2021	0	0	0	0	0	0

* = Cut-off occurred

CHAPTER THREE:

THE HYDROLOGIC AND GEOMORPHIC DRIVERS OF FLOOD HAZARD ON THE ASSINIBOINE RIVER, SOUTHWESTERN MANITOBA, CANADA

3.1. Introduction

Floods are the most frequent natural disaster in Canada, particularly in the prairies, and are caused by hydro-meteorological conditions that exceed a rivers ability to convey resulting discharge (Burn et al., 2016; Gaur et al., 2019). It has been proposed that a recent increase in floods in the prairies is the result of climate change (Simonovic & Li, 2004; Rasmussen, 2015; Burn et al., 2016; Gauer et al., 2019), and this notion has become a part of public discourse (e.g., Dacey & Thompson, 2021; Caruk, 2022). Nonetheless, it has been difficult to confidently prove a connection between climate change and alterations of the flood regime in the prairies (Simonovic & Li, 2004; Rasmussen, 2015; Burn et al., 2016; Gauer et al., 2019). However, these studies, much like infrastructure and insurance, only consider the contribution of river discharge and climatic inputs to the flood hazard (Shrubsole et al., 2003; Co-operators, n.d.). More recently, bathymetric data has become part of flood risk assessment (Ohio-Kentucky-Indiana Water Science Center, 2016; Natural Resources Canada [NRC], 2022). Flooding occurs when the discharge upstream exceeds the capacity of the channel at flood stage, and the number of days per year that this occurs is termed 'flood hazard frequency'. An increase in flood frequency may result from an increase in discharge as a result of climatic inputs or a decrease in channel capacity due to in-channel sedimentation (i.e., channel-bed aggradation) or decrease in slope (e.g., isostatic rebound). Therefore, it is important to evaluate the contributing factors (i.e., climate vs capacity) to flood risk to understand driving factors in future flood events and properly manage flood mitigation strategies.

Five of the ten largest floods on record have occurred since 1996 on the Red and Assiniboine Rivers, leading to the investigation of whether recent flooding events are the result of climate change (Fig. 3.1; GOM, n.d.; Simonovic & Li, 2004; Blais et al., 2016a; Rasmussen,

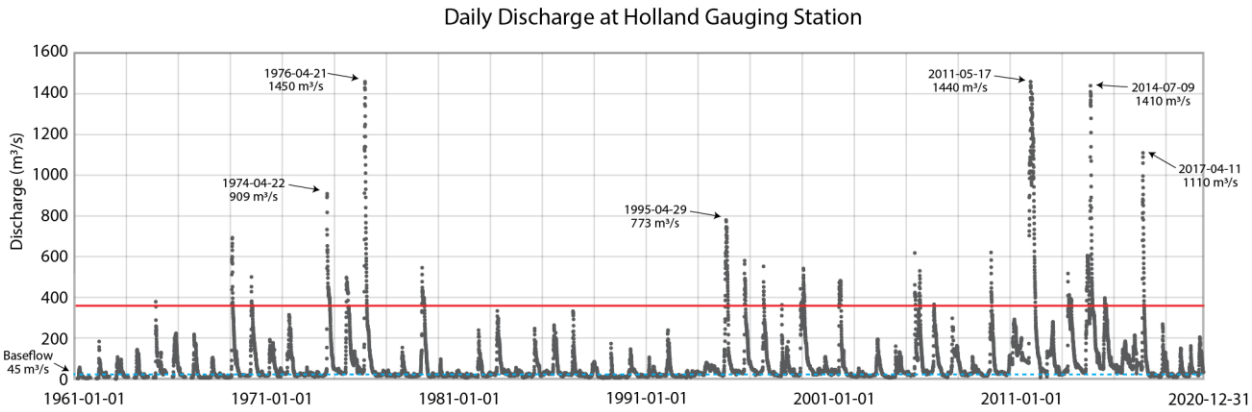

Daily discharge of the Assiniboine River at the Holland Gauging Station (Station 05MH005) from 1961 to 2020. The six largest flows since observation began are indicated (1974, 1976, 1995, 2011, 2014, and 2017). Baseflow (45 m3/s) is indicated by the dashed blue line and moderate flood stage (364 m3/s) is indicated by the red line

2015; Burn et al., 2016; Gauer et al., 2019). Studies on the impact of climate change on floods on the Red River indicate a range of possibilities. Simonovic and Li (2004) found that based on models of future climate change, there may be an increase in annual discharge and floods would both begin and peak earlier in the year than at present. Rasmussen (2015) concluded that snow accumulation in the winter is likely to decrease but rainfall during snowmelt is expected to increase. Their study suggests that change in flood regimes is likely to occur, however, variability in global climate models and emission scenarios made it difficult to conclude whether flood frequency would increase or decrease. In a study on flooding related to climate change and the impact specifically on flood infrastructure, Gaur et al. (2019) found that flood infrastructure in the prairies would experience the highest increases in future flooding frequencies. These studies only accounted for changes in flow frequencies contributing to an increase in flooding, yet research on changes in stream channel cross-sectional area altering local channel capacity (Stover and Montgomery, 2001; Lane et al., 2007) indicate that flow frequency may not be the only factor that can lead to a change in flood hazard (Slater et al., 2015). A reduction in channel cross-sectional area occurs through aggradation, the deposition of sediment within the active channel (Fig. 3.2). Even if the flow frequency distribution remains the same, reducing the accommodation for the same volume of water travelling at the same velocity raises water levels and increases the likelihood of overbank flooding.

The purpose of this study is to investigate the relative contribution of channel geomorphic change to the flood hazard on the Assiniboine River (Fig. 3.3). The Assiniboine River has been studied less than the Red River, however, it has experienced three extreme floods since 2010 (Fig. 3.1). The geomorphic change and resulting sedimentation caused by these extreme floods in Spruce Woods Provincial Park was studied in Chapter 2. Here, data and field measurements from

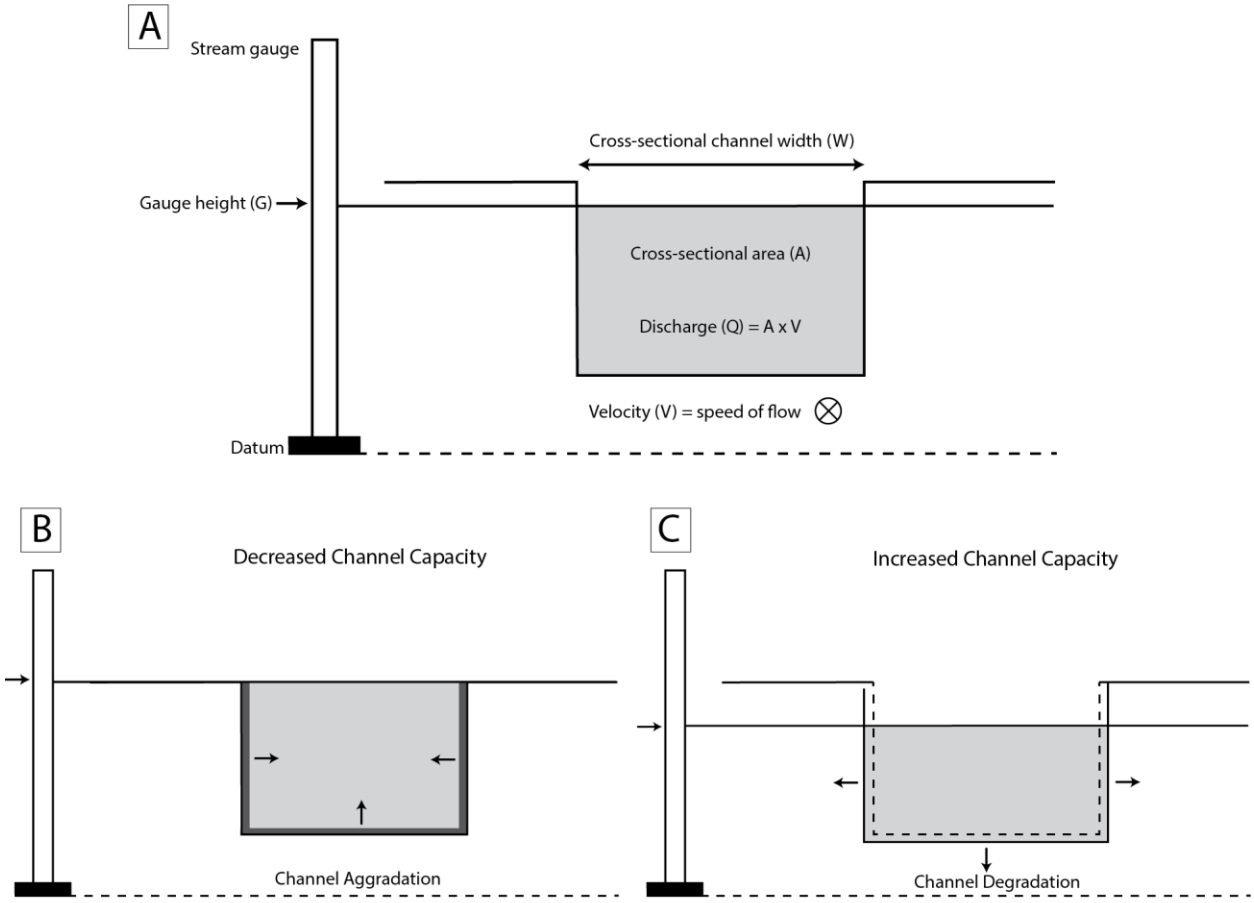

Fig 3.2. (A) Schematic of channel cross-section with stream gauge. (B) Schematic of channel aggradation, demonstrating decreased channel capacity and increase gauge height. Aggradation represented by dark grey polygons. (C) Schematic of channel degradation, demonstrating increased channel capacity and lowered stream gauge. Former channel is indicated by dashed line. Modified from Slater et al., 2015.

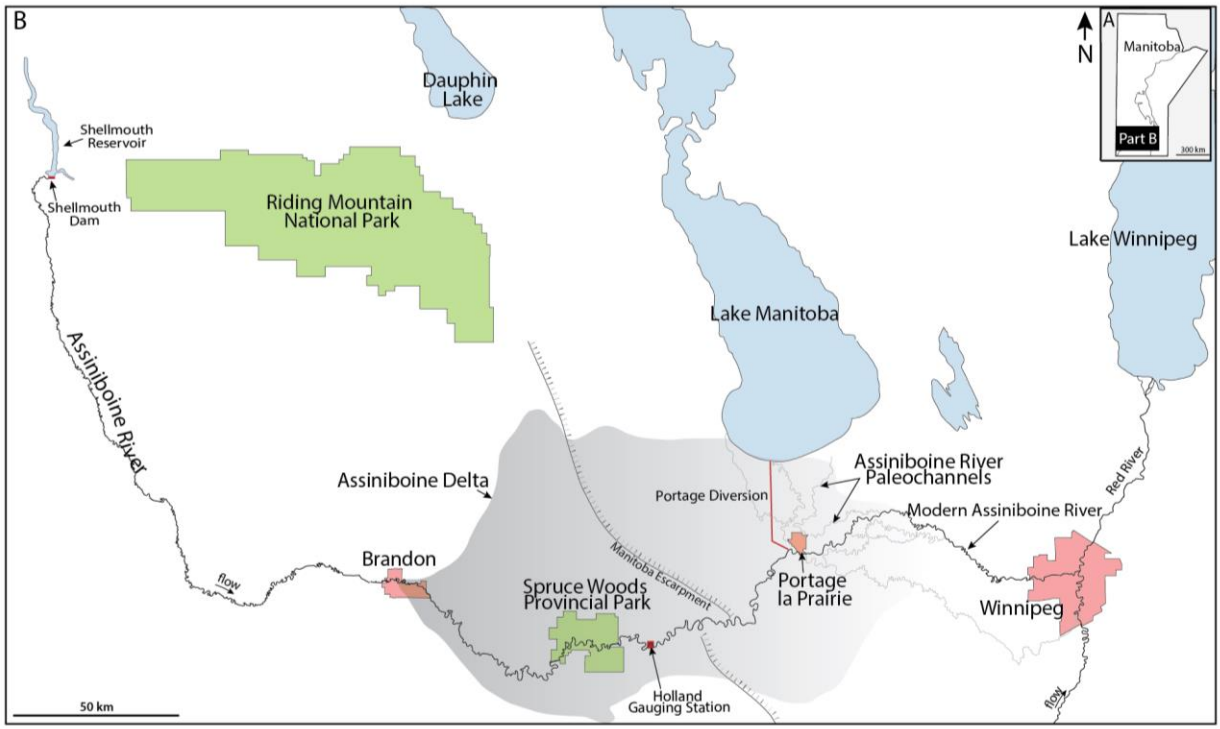

Fig. 3.3. (A) Map of Manitoba. (B) Assiniboine River from the Shellmouth Dam to the city of Winnipeg. The Shellmouth Reservoir, Shellmouth Dam, and Portage Diversion are indicated. (C) Satellite image (ESRI, 2018) of the Holland Gauging Station location.

from a gauging station 50 km downstream of the study area are analysed to assess the relative contribution of hydrological and sedimentological factors to flood hazard on the Assiniboine River (Fig. 3.1). Further downstream, beyond Portage La Prairie, the Assiniboine River has a long avulsion history, a process that is driven by aggradation and construction of alluvial ridges, indicating channel aggradation has occurred on and may still be a risk on the Assiniboine River (Rannie et al., 1989; Törnqvist & Bridge, 2002). Results of this chapter will contribute to improving our understanding of the drivers of extreme floods, enabling better prediction of future floods and their potential impact on infrastructure surrounding the Assiniboine River.

3.2. Background & Study Area

The Assiniboine River valley was formed by glacial meltwater and drainage of proglacial lakes during deglaciation approximately 12,000 years ago (Klassen, 1972). The river can be divided into the upper and lower Assiniboine River. The study area and gauging station used in this research is on the upper Assiniboine River, upstream of Portage la Prairie, which erodes into sediment from the late glacial Assiniboine Delta forming a confining valley (Fig. 3.3; Fenton, 1970; Kehew and Teller, 1993; Boyd, 2007). The lower Assiniboine River, downstream of Portage la Prairie, emerges from the confined valley of the Assiniboine delta and migrates freely on the nearly flat plain of the former glacial Lake Agassiz (Rannie et al., 1989). Starting just west of Portage la Prairie, the river has built a large, low-angle alluvial fan (Rannie, 1990). This fan was constructed through multiple avulsions of the Assiniboine River over the course of the last 7000 years (Rannie et al., 1989; Rannie, 1990). The initial course of the Assiniboine River was north into Lake Manitoba; beginning ~3,000 years ago, a series of avulsions caused by continued alluviation altered the course eastward towards the Red River (Rannie et al., 1989).

The Assiniboine River first connected with the Red River 14 km south of its current confluence, along the present course of the La Salle River (Rannie et al., 1989). Further aggradation on the fan caused the Assiniboine River to avulse three more times to establish its present course (Rannie et al., 1989). The Holocene avulsion frequency is approximately every 875 years, and the most recent avulsion occurred 700 years before present (Rannie et al., 1989)As the distribution of flow frequencies is controlled by climatic factors, it is important to understand the causes of high discharge events. The 2011 Assiniboine River flood was the largest ever recorded in the more than 100 years of observation of the Assiniboine River. Conditions leading to the 2011 flood began in the fall of 2010 where high soil moisture at freeze-up followed by above normal snowfall and lower than normal temperature during the winter of 2010/2011 resulted in deep frost penetration (GOM, 2013). The combination of high soil moisture and deep frost penetration reduced the soil's ability to absorb spring meltwater. This was further exacerbated by unprecedented rainfall volumes in the spring of 2011, culminating in extensive flooding that lasted for 120 days (GOM, 2013). At the Holland gauging station, the 2011 flood had a calculated return period of 350 years with a peak flow of 1440 m^3/s (Blais et al., 2016b).

The 2011 flood was unprecedented due to its extreme discharge whereas the 2014 flood was unprecedented as it was the first summer flood in the history of the Assiniboine River. In the summer of 2014, the spring freshet had already passed, and flows had returned to baseflow (Ahmari et al., 2016). Although the spring freshet had not caused flooding, it was still an extremely wet period with saturated soil (Ahmari et al, 2016). Therefore, when the Assiniboine River basin experienced multiple rain-fall events that were up to 200% above average, the river experienced yet another "unprecedented flood" in the summer generated solely by precipitation (Ahmari et al., 2016). The 2014 flood had a peak flow of with 1440 m^3/s at the Holland gauging

station and an estimated return period between 200 to 400 years, although measuring the exact probability is difficult as it is the first summer flood to occur during human observation of the Assiniboine River (Ahmari et al., 2016).

The Assiniboine River once again experienced extreme discharge in the spring of 2017 with a peak flow of 1100 m^3/s at the Holland gauging station. Using the hydrograph produced by Ahmar et al., (2016) and the peak flow of 1040 m^3/s at the associated gauging station (Assiniboine River near Brandon, station 05MH013), this flood had a return period of approximately 200 years. This flood was the result of a warmer fall that delayed freeze-up and resulted in record high flows for the time of year ([Manitoba[Hydrologic Forecast Centre, 2016). Fortunately, a very dry spring and flood infrastructure mitigated the severity of the 2017 flood (Manitoba Sustainable Development, 2018). Since 2017, the flows on the Assiniboine have ranged from low baseflow (i.e., 2019) to moderate flooding with some overbank flow in low-lying areas (i.e. 2022).

The Holland Gauging Station (Station 05MH005) is located north of Holland, Manitoba at a bridge crossing on Provincial Trunk Highway 34. The bridge bisects a point bar on the upstream limb. It is 280 km downstream of the Shellmouth Dam and 65 km upstream of the Portage Diversion, limiting anthropogenic alterations of flow as much as possible. At this location, the Assiniboine River's drainage basin is approximately 160,000 km^2, or 99% of its total drainage basin. Baseflow is 46 to 53 m^3/s and peak discharge is typically in April or May, occasionally in July. This gauging station was selected for the study because of its proximity to Spruce Woods Provincial Park (Chapter 2), relatively limited anthropogenic alteration, and the large extent of the drainage basin it captures.

3.3. Methods

This study uses continuous flow gauge data collected from 1967 to present day (2022). Due to how discharge is calculated from water level, regular field measurements have been taken at the gauging site since 1995 that record discharge, water velocity, stage, and area of the channel (Environment and Climate Change Canada, n.d.). These measurements calibrate the stage-discharge curve that calculates discharge from the water level registered at the gauging station. In this study, daily discharge values and field measurements are used to calculate the relative contribution of flow frequency and channel change to flood hazard over time. Flood stage is assumed to remain constant at 296.95 m. a. s. l. as stated by the Manitoba Hydrologic Forecasting and Water Management in the Forecast/Flood Sheets (2022). Using a constant flood stage allows for the quantification of temporal changes in discharge required to reach flood stage.

The measurement of changes in channel capacity are based on field measurements, therefore various filtering steps were taken to ensure the values used in calculations were accurate. Any measurements collected during icy conditions were discarded as it reduces the river cross-section and produces an anomalously higher river stage for a given discharge than would occur without the presence of ice. Any entry that was missing a discharge, area, or velocity value was removed for consistency. The data was then tested for accuracy by measuring the ratio of discharge to velocity and area; any ratio that was greater than or less than 1 by a margin greater than 1% was omitted. Finally, as this research pertains to changes occurring at flood stage, the data used was limited to field measurements at or near flood stage, spanning a range of values plus or minus a range of half the channel depth at flood stage.

The basis of this research is that the flood hazard frequency may be altered either by a change in flow or by a change in channel capacity (e.g. Slater et al., 2015). To test the impact that one factor has on the flood hazard frequency, the other factor is held constant. First, the average discharge, average velocity, and average area at flood stage were calculated using the field measurement data. The field-measurement based natural logarithm of discharge, velocity, and area were respectively graphed against the natural logarithm of stage (Fig. 3.4). Each graph was fit with a least square regression line from which the average value at flood stage was derived.

The first flood hazard frequency factor measured was of the 'flow frequency effect': the change in flood frequency that would occur as a result of changes in flow frequency when channel capacity is held constant. This measures the climatic effect on flooding as a change in flow frequency occurs due to a change in discharge (i.e. an increase in discharge resulting from an increase in precipitation, and/or an increase in the amount of precipitation that discharges into the river). To do this the number of days per year that was equal to or greater than a given threshold was plotted for every year with continuous discharge data. Typically, the threshold used is the discharge at flood stage as calculated from field measurements. However, this value (970 m^3/s) was not used in this study as it was skewed by the data only dating back to 1995. This threshold would omit some of the Assiniboine River's peak flow events (i.e., 1974, 1975, 1995, 1996, and 2009). The mean maximum discharge recorded annually over the period of observation was used instead – 364 m^3/s. This value was chosen as it captures the peak flow events that have occurred over the period of observation at this gauging station. For the purpose of this paper the threshold will be termed "moderate flood stage". The graph was fit with a mean

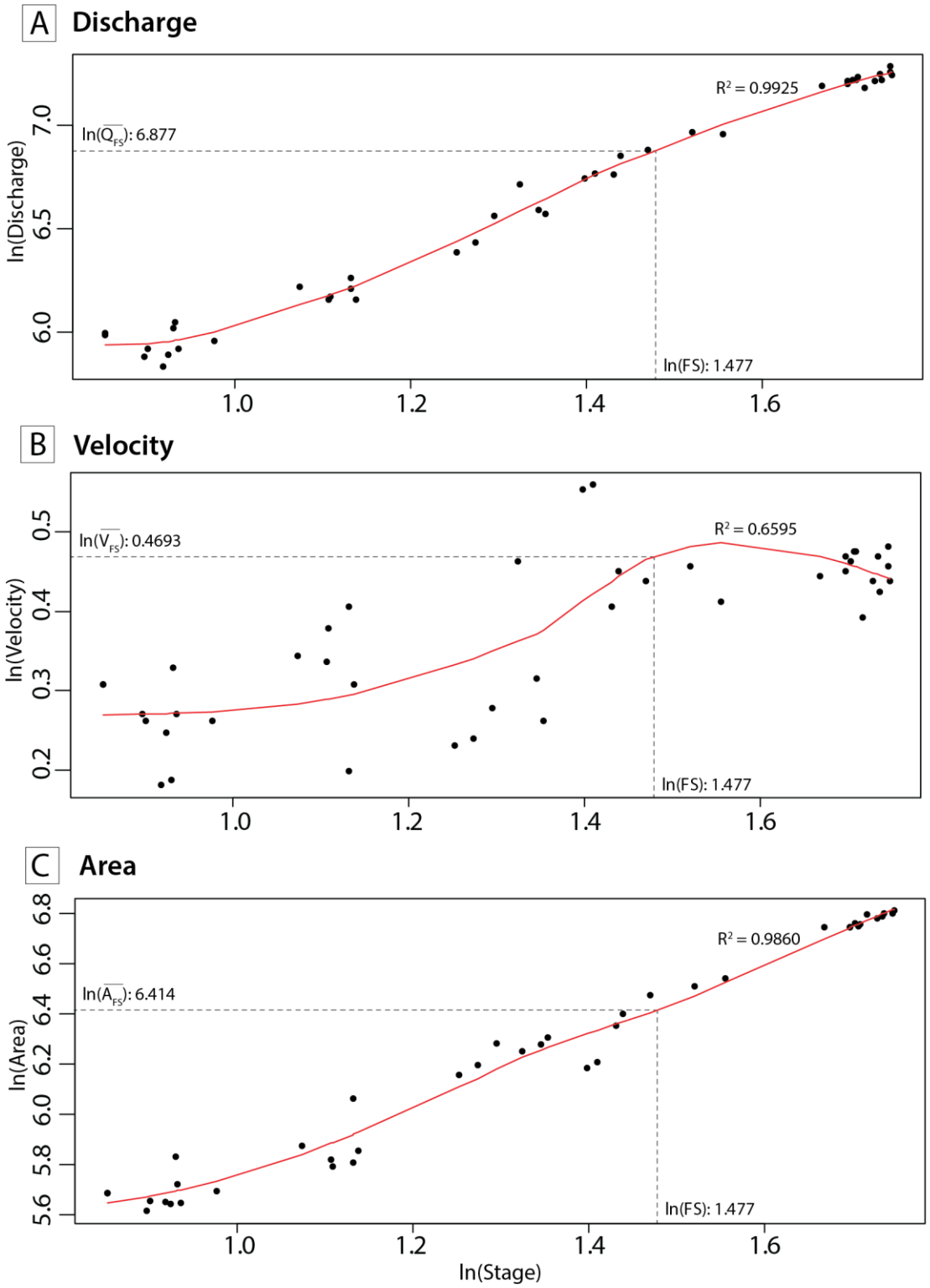

Fig 3.4. (A) Discharge rating curve. Discharge at flood stage (FS) is indicated. (B) Velocity rating curve. Velocity at flood stage is indicated. (C) Area rating curve. Area at flood stage is indicated.

unbiased exponential least squares curve to prevent predicting negative values. This curve indicated the percent change per decade that had occurred since observation began.

The second factor to be quantified was the 'channel capacity effect'; the change to flood hazard frequency that would occur from shifts in channel capacity if the flow frequency distribution was constant. As field measurements are rarely made exactly at flood stage, it was necessary to calculate what discharge would be at flood stage when each measurement was taken. To do so, the natural logarithm of discharge was plotted against the natural logarithm of gauge height (Fig. 3.5a). This graph was then fit with a least square regression line. The difference between observed discharge and the estimated discharge from the loess curve (the residuals) was added to the average discharge at flood stage (970 m^3/s) to determine what discharge would have been at flood stage (Fig. 3.5a). These discharge values were then plotted on the frequency curve created for this gauging station using the daily stream flow values to determine the days per year this discharge is reached (Fig. 3.5b). Then, these values were used to illustrate the channel change capacity occurring annually. The contribution to flood hazard frequency can then further be broken into the velocity and area component due to the field measurements taken. Similarly, the estimated velocity and cross-sectional area of each field measurement are taken from a loess curve fit to the actual measurements and the residuals are then added to the average velocity at flood stage and the average area at flood stage to estimate what the velocity and area were at flood stage when the field measurements were taken. Finally, these values are plotted over time to see what change has occurred during the period of observation. A Mann-Kendall test was used to test the significance of the results.

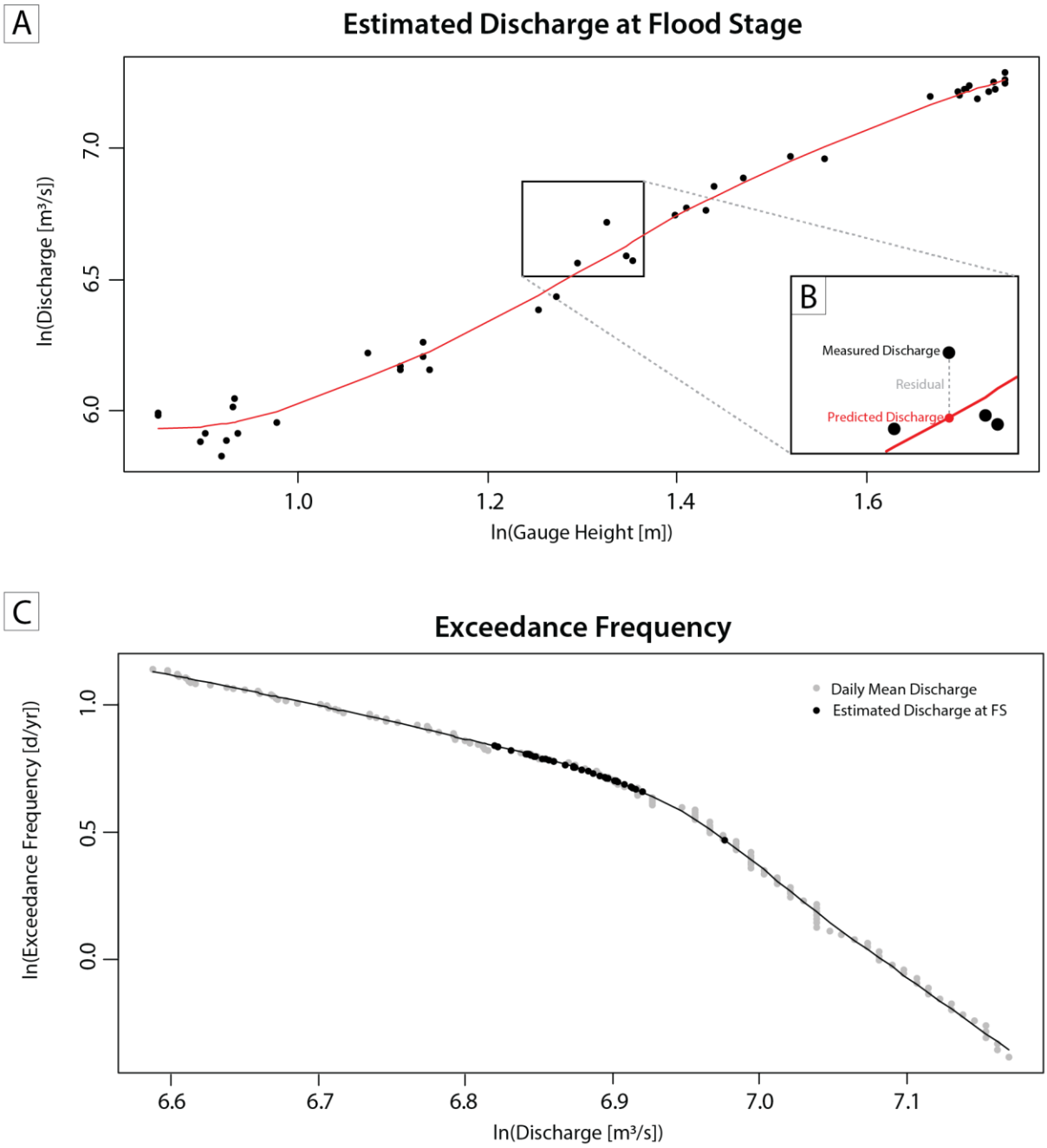

Fig. 3.5. (A) Rating curve of discharge. (B) The residual is the differences between measured discharge (black circle) and predicted discharge (red line). (C) Exceedance Frequency in days per year of daily mean discharges (light grey circles). The Exceedance Frequency of the estimated discharges (black circles) is derived from the black trend line.

3.4. Results and Analysis

Over the 53 years of daily discharge data collected at the Holland Gauging Station, the number of days exceeding moderate flood stage has increased by 18% per decade (Fig. 3.6). The 1970s had two of the peak flow events on record for the Assiniboine River, 1975 and 1976, with two more years, 1974 and 1979, experiencing more than 40 days of moderate flooding. The 1980s did not record a day of moderate flooding. The first half of the 1990s continued to have no days of moderate flooding but every year from 1995 to 1999 recorded at least one day of moderate flood stage. In 1995, one of the strongest peak flow events ever recorded occurred on the Assiniboine River. From 2000 to 2009, six year did not record a day at or over moderate flood stage. The 2010s' contained three of the highest discharge events on record (2011, 2014, and 2017) and two additional years that reached or exceeded moderate flood stage. Based on the data available, it appears that moderate flood stage was reached more frequently following 1995. Using the Mann-Kendall test, which tests for a monotonic upward or downward trend over time, there was no significant trend found for this data. This is likely due to the large variability and relatively short human record of observation. It is also important to note that this measurement of flow frequency does not give a full picture of changes that are occurring with river flow and emphasizes duration of flood events without considering the differences in peak discharge. For example, 2013 and 2017 had a similar number of days of moderate flooding but 2013 had a peak discharge of 518 m^3/s, less than half of 2017's peak discharge of 1110 m^3/s.

Flow frequency is also impacted by the channel capacity, which has slightly decreased the flow frequency at a rate of -3.0% per decade (Fig. 3.7a). The Mann-Kendall test showed a significance ($p < 0.05$) to this trend. Changes in channel capacity are the result of changes to velocity of the flow and cross-sectional area of the channel. From 1995 to 2020, velocity at flood

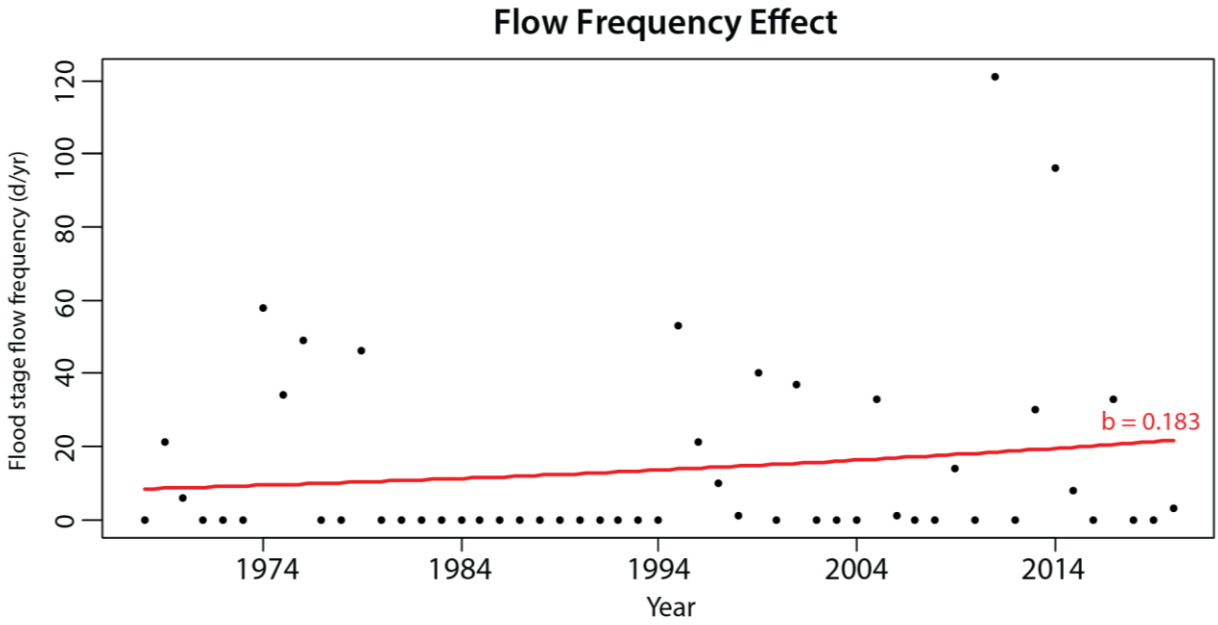

Fig 3.6. Change in flow frequency from 1961 to 2020. Black circles represent the days per year at or above moderate flood stage. The trend is indicated by the red line (18% per decade). A Mann-Kendall test indicates that this is not a statistically significant trend.

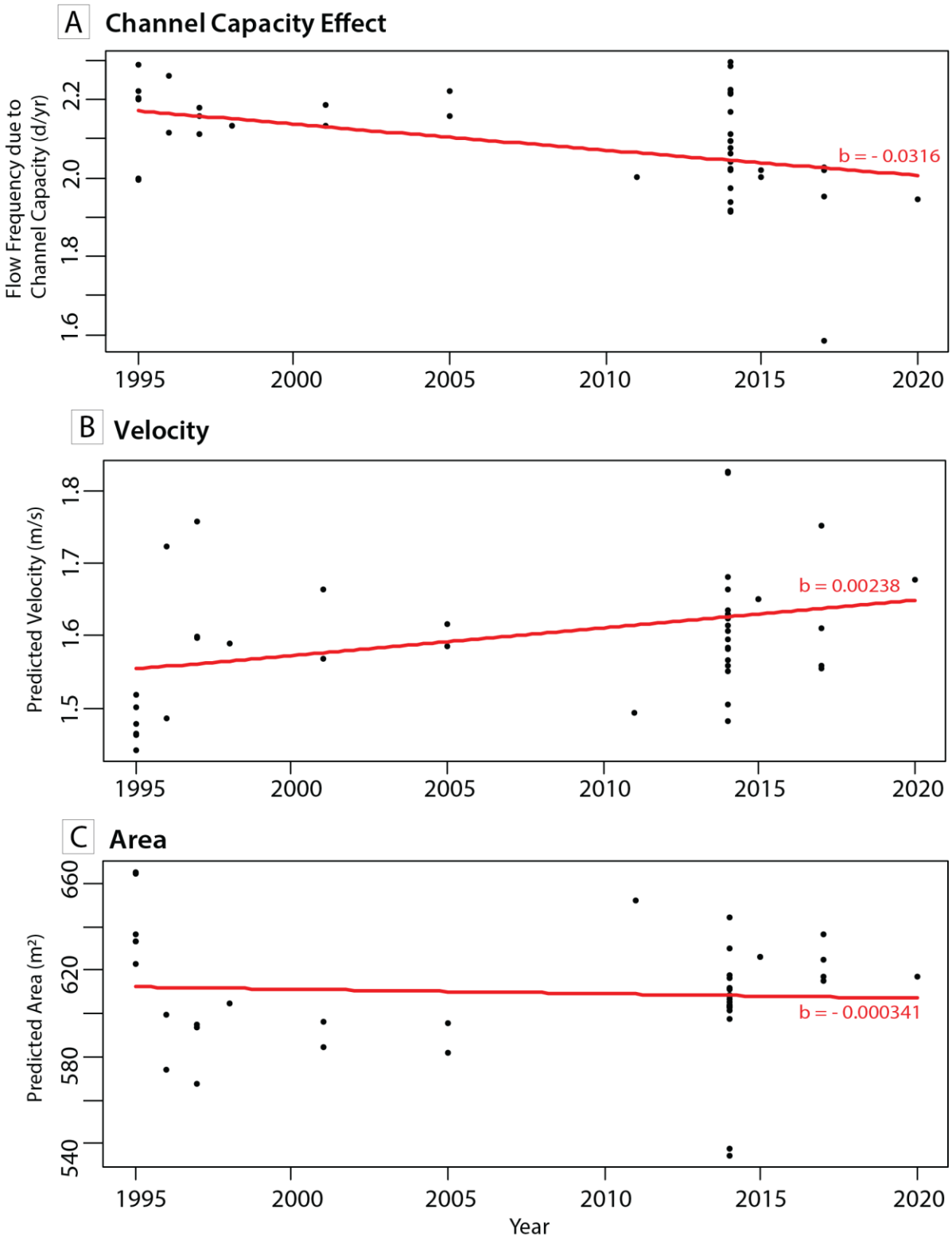

Figure 3.7. (A) Change in channel capacity from 1995 to 2020. The red line is the trend (-3.0 % per decade) and it is statisitcally significant ($p < 0.05$). (B) Change in velocity from 1995 to 2020. The red line is the trend (+0.2 % per decade) and it is not statisitically significant. (C) Change in cross-sectional area from 1995 to 2020. The red line is the trend (-0.03 % per decade) and it is not statistically significant.

stage increased 0.2% per decade while area at flood stage decreased 0.03% per decade resulting in a minor decrease in flow frequency due to channel capacity (Fig. 3.7b, c). Changes in velocity result from changes in slope and cross-sectional area of the channel (Julien, 2002). The slope in this region is very gentle, 0.0005, and isostatic rebound following deglaciation is minimally reducing the gradient over time, thus, the increase in velocity at flood stage is likely a result of the observed decrease in area (Fig. 3.7b; Brooks et al., 2005; Blais et al., 2016b).

Although there is a significant trend in the change in channel capacity, the trends measured for velocity and area were not significant, were within error, and therefore, negligible. Both the predicted velocity at flood stage and the predicted area at flood stage had variations in their data sets that made it difficult to derive a significant trend. There were several years with no useable velocity and area measurements (i.e., 2006 – 2010) and several years with multiple measurements that had great variability in their predicted velocity and area at flood stage (i.e., 2014). Ultimately, at the study site, the flow frequency effect was greater than that of the channel capacity effect, despite the inability to find a significant trend in the flow frequency data.

3.5. Discussion

The increase in flow frequency is related to an increase in discharge. Moderate flood discharges are being reached at an increased rate and typically persist for 20 to 40 days. Discharge increases due to increases in precipitation (Vinet, 2017). However, flooding is not solely driven by precipitation. For instance, in Manitoba, flooding is impacted by soil moisture at freeze-up, the winter snowpack, snow and rain during the spring freshet, and summer rainfall (Blais et al., 2016b; Berghuijs et al., 2016). All these factors are controlled by climate. As stated previously in studies attempting to connect flooding to climate change, it is difficult to prove the

observed changes in flow frequency are related to shifts in the climate; however, it has become increasingly evident there has been change in climate of the Canadian prairies (IPCC, 2022). According to the Intergovernmental Panel on Climate Change (IPCC), warmer temperatures lead to an increase in precipitation and reduction in snowpack. Across the Canadian prairies, where the Assiniboine River's basin lies, there has been an observed change in temperature from 1980 to 2015 between -0.2°C and +0.3°C per decade (IPCC, 2022). With a 2°C increase in global temperature, average annual temperatures in this region are predicted to rise 1°C to 2°C (IPCC, 2022). With a 4°C increase in global temperature, temperatures in this region are predicted to rise 5°C to 6°C (IPCC, 2022). Furthermore, there is expected to be in increase in the intensity of local heavy precipitation, with a greater proportion of precipitation occurring in intense events due to warming in this region (IPCC, 2022). The result of intense rainfall events can be seen in the 2014 flood, the only summer flood on record for the Assiniboine River. Whereas Assiniboine River flooding is typically the result of depth of frost penetration, the winter snowpack, spring freshet and precipitation, the 2014 flood was solely driven by intense precipitation events.

Another potential cause of increased river discharge is anthropogenic change occurring in the river basin (i.e., monoculture agriculture and urbanization) that increases runoff, resulting in higher discharge (Galster et al., 2006; Sommerville & Magnan, 2015). Since the 1980s, farms on the prairies have increasingly been sold to land investors, shifting agriculture towards monoculture production (Sommerville & Magnan, 2015). High-input farming results in increased soil erosion and increased run-off (Parr et al., 1990). The crops commonly used in monoculture farming (i.e., corn and soybeans) do not have roots that are as deep as native prairie vegetation therefore there is less soil cohesion and connectivity with the water table (Schulte et al., 2017). Additionally, the population in Manitoba has increased from 1,026,241 people in 1981 to

1,342,000 people in 2021 (Statistics Canada, 1981; Statistics Canada, 2022). Over that same period of time, the population of Brandon, the largest city upstream of the study area (approximately 65 km upstream), has increased from approximately 38,000 people to approximately 51,000 (Statistics Canada, 1981; Statistics Canada, 2022). As the urban population increases, so does the extent of the city. The change in land-use creates more impervious surfaces, leading to an increased volume of discharge delivered to the river at a faster rate (Galstter et al., 2006).

The increase in channel capacity is due to an increase in velocity. The increase in velocity is most likely driven by the decrease in the channel's cross-sectional area, indicating cross-sectional area is the main control of channel capacity. Although the trend for changes in velocity and cross-sectional area were insignificant, the channel capacity trend was significant; thus, it is important to understand how the channel capacity is changing locally. Channel cross-sectional area decreases due to deposition of sediment within the channel (i.e. aggradation). There are several potential causes for channel aggradation – changes in discharge, river morphology, sediment load, and post-glaciation isostatic rebound (Mugade & Sapkale, 2015). Aggradation due to changes in discharge typically results from a decrease in discharge wherein the energy of the flow is unable to convey the bedload or suspended sediment. As shown by the increase in flow frequency, this is unlikely to be the cause of aggradation in this area of the river because discharge has increased over time. The morphology of the river, in particular the presence of riparian vegetation and aquatic plants, also plays a significant role in river aggradation (Mugade & Sapkale, 2015). There is a strong correlation between vegetation and trapping sediment in the channel (Gurnell et al., 2012). In the study area, there are numerous large, unvegetated point bars and the vegetation that is visible in satellite imagery is several meters above the channel on

erosional bluffs (Fig. 3.1; Ashmore, 1992). Thus, it is unlikely aggradation is occurring due to sediment trapped by vegetation and in fact, this topography likely increases the sediment load of the Assiniboine River through slumping and spring sapping (Wolowich & Tamburi, 1985; Ashmore, 1992). At the gauging station used for this study there is no measurement of sediment loads and studies documenting sediment yields for the Assiniboine basin report very low sediment loads compared with other prairie drainage basins (Ashmore, 1990; Ashmore, 1992). However, the highest sediment loads for the region were recorded in the central region of the river, where the gauge for this study is located (Ashmore, 1992). The most likely cause of change to channel capacity is a decrease in channel cross-sectional area due to sediment loads that are too high to convey.

Additionally, long-term aggradation can lead to avulsion (Jones and Schumm, 1999). Avulsion, the displacement of a river channel, occurs when a channel near its stability threshold experiences a triggering event, typically a flood (Jones & Schumm, 1999). As a river approaches its stability threshold, it requires a decreasing magnitude discharge event to trigger an avulsion. There are several factors that are typically combined to cause a river to reach its threshold: a decrease in gradient of the existing channel, an increase in gradient away from the existing channel, and a reduction in the channel capacity (Jones and Schumm, 1999). The studied region of the river is partially confined, whereas downstream of Portage la Prairie the river becomes unconfined and, as previously described, has a long history of avulsion.

Flow frequency has a greater contribution to the flow hazard frequency, yet the factors driving flow frequency are difficult to control. Significant work has been done in Manitoba to construct infrastructure to mitigate the impact of extreme floods on the Assiniboine River (i.e., the Shellmouth Dam, the Portage Diversion, levees, etc.). Addressing channel aggradation, with

methods such as dredging, is a feasible solution that can be more readily implemented. Increasing the area of the channel will increase the channel's capacity, increasing accommodation for high discharges, and lower the potential for an avulsion event to occur. For instance, local dredging has been utilized on the Mississippi River for flood mitigation (i.e. Pinter et al., 2004).

Ultimately, the results of this study are not exhaustive and are meant as a first step to identify the factors contributing to the recent increase in flooding on the Assiniboine River. There was a significant trend in the change in channel capacity, indicating that flow frequency is not the sole driver of flooding in this area. It is worthwhile to further investigate changes occurring to the river locally, such as aggradation, to investigate whether smaller-scale local adaptations can be made to reduce flood hazard. Future work on this subject should incorporate more gauging stations to understand what is happening to the channel's capacity over the entire length of the river. Additionally, extending the timescale and the number of the field measurements used in this research would yield a more accurate analysis of the trends that effect channel capacity.

3.6. Conclusions

This study quantifies the change in flow frequency and the change in channel capacity that are contributing to flood hazard frequency on the Assiniboine River. This was achieved using continuous flow gauge discharge measurements from 1967 – 2020 and field measurements from the gauging station from 1995 – 2020. The data was analyzed using statistical analysis to try and detect a significant trend occurring to flow frequency and channel capacity over the period of observation. The main driver of flooding appears to be the flow frequency, increasing

18% per decade. A significant trend in channel capacity indicates that it also influences flood hazard frequency. In the instance of the Holland Gauging Station, channel capacity is decreasing the flow frequency 3.0% per decade. The results indicate that to accurately quantify the hazard of future flood events, discharge and channel capacity must both be considered. Furthermore, this indicates there is an opportunity for a more localized approach to flood mitigation strategies. Although the precise cause of the change in channel capacity could not be identified, future work may further improve our understanding of flooding on the Assiniboine River.

3.7. References

Ahmari, H., Blais, E-L. and Greshuk, J. (2016). The 2014 flood event in the Assiniboine River Basin: Causes, assessment, and damages. *Canadian Water Resources Journal, 41*(1-2), 85-93.

Ashmore, P.E. (1990) Analysis and interpretation of Assiniboine River sediment station data. Inland Waters Directorate, Water Resources Branch, Western and Northern Region.

Ashmore, P. E. (1992) Sediment delivery in large prairie river basins, western Canada. Erosion and Sediment Transport Monitoring Programmes in River Basins, 423-432.

Berghuijs, W. R., Woods, R. A., Hutton, C. J., & Sivapalan, M. (2016). Dominant flood generating mechanisms across the United States. *Geophysical Research Letters*, *43*(9), 4382-4390.

Blais, E. L., Clark, S., Dow, K., Rannie, B., Stadnyk, T., & Wazney, L. (2016a) Background to flood control measures in the Red and Assiniboine River Basins. *Canadian Water Resources Journal*, *41*(1–2), 31–44.

Blais, E-L., Greshuk, J. and Stadnyk, T. (2016b). The 2011 flood event in the Assiniboine River Basin: Causes, assessment, and damages. *Canadian Water Resources Journal*, *41*(1-2), 74-84.

Brooks, G. R., Thorleifsonl, L. H., & Lewis, C. M. (2005). Influence of loss of gradient from postglacial uplift on Red River flood hazard, Manitoba, Canada. *The Holocene*, *15*(3), 347-352.

Caruk, H. (2022, May 14) Is Manitoba's wild weather a sign of climate change? *CBC News*. https://www.cbc.ca/news/canada/manitoba/climate-change-manitoba-prairies-weather-1.6447990#:~:text=While%20variability%20is%20the%20norm,swings%20more%20extreme%2C%20experts%20say&text=Trevor%20Brine%2FCBC)-,Within%20the%20span%20of%20a%20year%2C%20Manitoba%20went%20from%20having,its%20worst%20floods%20on%20record.

Co-Operators. (n.d.*) How do we determine flood risk?* Retrieved August 2, 2022 from https://www.cooperators.ca/en/Resources/protect-what-matters/determining-flood-risk.aspx

Dacey, E. & Thompson, S. (2021, August 10) Climate change in our backyard: Manitoba begins to grapple with the consequences. *Global News.* https://globalnews.ca/news/8097926/climate-change-consequences-manitoba/

Esri. (July 17, 2018). World Topographic Map. http://www.arcgis.com/home/item.html?id=30e5fe3149c34df1ba922e6f5bbf808f (Accessed October 29, 2022).

Environment and Climate Change Canada (n.d.) *Frequently Asked Questions*. Retrieved Oct 2022 from: https://wateroffice.ec.gc.ca/contactus/faq_e.html

Galster, J. C., Pazzaglia, F. J., Hargreaves, B. R., Morris, D. P., Peters, S. C., & Weisman, R. N. (2006). Effects of urbanization on watershed hydrology: The scaling of discharge with drainage area. *Geology*, *34*(9), 713-716.

Gaur, A., Gaur, A., Yamazaki, D., & Simonovic, S. P. (2019) Flooding related consequences of climate change on Canadian cities and flow regulation infrastructure. *Water (Switzerland)*, *11*(1). https://doi.org/10.3390/w11010063

Government of Manitoba [GOM]. (n.d.a) History of Flooding in Manitoba. Retrieved June 2022 from: https://www.gov.mb.ca/flooding/history/index.html#:~:text=Manitoba%20Flood%20Facts,River%20and%20Assiniboine%20River%20basins.

Government of Manitoba [GOM]. (n.d.b) Historic Floods. Retrieved August 2022 from: https://www.gov.mb.ca/mit/wms/floodcontrol/arbasin/historic.html#:~:text=ZIP%2C%2014%20MB)-,1976,since%20the%20flood%20of%201882

Government of Manitoba [GOM]. (2013) Manitoba 2011 Flood Review Task Force Report: Report to the Minister of Infrastructure and Transportation. Retrieved June 2022 from: https://www.gov.mb.ca/asset_library/en/2011flood/flood_review_task_force_report.pdf

Gurnell, A. M., Bertoldi, W., & Corenblit, D. (2012). Changing river channels: The roles of hydrological processes, plants and pioneer fluvial landforms in humid temperate, mixed load, gravel bed rivers. *Earth-Science Reviews, 111*(1-2), 129-141.

Hamilton, A. S. and Moore, R. D. (2012) Quantifying Uncertainty in Streamflow Records. *Canadian Water Resources Journal, 37*(1).

Horner, I., Renard, B., Le Coz, J., Branger, F., McMillan, H. K., & Pierrefeu, G. (2018) Impact of stage measurement errors on streamflow uncertainty. *Water Resources Research*, *54*(3), 1952-1976.

IPCC, 2022: *Climate Change 2022: Impacts, Adaptation, and Vulnerability.* Contribution of Working Group II to the Sixth Assessment Report of the Intergovernmental Panel on Climate Change [H.-O. Pörtner, D.C. Roberts, M. Tignor, E.S. Poloczanska, K. Mintenbeck, A. Alegría, M. Craig, S. Langsdorf, S. Löschke, V. Möller, A. Okem, B. Rama (eds.)]. Cambridge University Press. In Press

Jones, L. S., & Schumm, S. A. (1999). Causes of avulsion: an overview. *Fluvial sedimentology VI*, 169-178.

Julien, P. Y. (2002). *River Mechanics*. Cambridge University Press.

Lane, S. N., Tayefi, V., Reid, S. C., Yu, D., & Hardy, R. J. (2007) Earth Surface Processes and Landforms Earth Surf. *Earth Surf. Process. Landforms*, *32*, 429–446. https://doi.org/10.1002/esp

Pinter, N., Miller, K., Wlosinski, J. H., & van der Ploeg, R. R. (2004). Recurrent shoaling and channel dredging, Middle and Upper Mississippi River, USA. *Journal of Hydrology*, *290*(3-4), 275-296.

[Manitoba] Hydrologic Forecast Centre (2016) 2016 Fall Conditions Report. Retrieved August 2022 from: https://www.gov.mb.ca/asset_library/en/2016flood/2016_Fall_Conditions_Report_Final.pdf

Manitoba Hydrologic Forecasting and Coordinate Branch (2017) 2017 January Conditions Report. Retrieved August 2022 from: http://manitoba.mb.ca/asset_library/en/2017flood/january_conditions_report.pdf

[Manitoba] Hydrologic Forecast Centre (2017) March Outlook Report. Retrieved August 2022 from: https://www.gov.mb.ca/mit/floodinfo/pdf/2017/march_outlook_2017.pdf

Manitoba Sustainable Development (2018) 2017 Water Availability and Drought Conditions Report. Retrieved August 2022 from: https://www.gov.mb.ca/sd/water/pubs/water/drought/2017/annual_summary2017.pdf

Mueller, D. S., Abad, J. D., García, C. M., Gartner, J. W., García, M. H., & Oberg, K. A. (2007). Errors in acoustic Doppler profiler velocity measurements caused by flow disturbance. *Journal of hydraulic Engineering*, *133*(12), 1411-1420.

Mugade, U. R., & Sapkale, J. B. (2015) Influence of aggradation and degradation on river channels: a review. Int. J. of Engineering and Technical Research, 3(6), 209-212.

Natural Resources Canada [NRC]. (2018) Federal Flood Mapping Framework, Version 2.0. Natural Resources Canada General Information Product 112e, Government of Canada, doi.org/10.4095/30812.

Natural Resources Canada [NRC]. (2022) Data related to flood mapping. Retrieved August 2, 2022 from https://www.nrcan.gc.ca/science-and-data/science-and-research/natural-hazards/data-related-flood-mapping/24250

Ohio-Kentucky-Indiana Water Science Center. (2016). Bathymetric Surveys. Retrieved December 11, 2022 from https://www.usgs.gov/centers/ohio-kentucky-indiana-water-science-center/science/bathymetric-surveys

Parr, J. F., Papendick, R. I., Youngberg, I. G., & Meyer, R. E. (1990). Sustainable agriculture in the United States. In *Sustainable agricultural systems* (pp. 50-67). CRC Press.

Pelletier, P. M. (1987) Uncertainties in the Single Determination of River Discharge: a Literature Review. *Canadian Journal of Civil Engineering, 5*(15).

Rannie, W. F., Thorleifson, L. H., & Teller, J. T. (1989) Holocene evolution of the Assiniboine River paleochannels and Portage la Prairie alluvial fan. *Canadian Journal of Earth Sciences, 26*(9), 1834-1841.

Rashid, H. (2011) Interpreting flood disasters and flood hazard perceptions from newspaper discourse: Tale of two floods in the Red River valley, Manitoba, Canada. *Applied Geography*, *31*(1), 35-45.

Rasmussen, P. F. (2016) Assessing the impact of climate change on the frequency of floods in the Red River basin. *Canadian Water Resources Journal*, *41*(1–2), 331–342. https://doi.org/10.1080/07011784.2015.1025101

Schulte, L. A., Niemi, J., Helmers, M. J., Liebman, M., Arbuckle, J. G., James, D. E., Kolka, R. K., O'Neal, M. E., Tomer, M. D., Tyndall, J. C., Asbjonsen, H., Drobney, P., Neal, J., Van Ryswyk, G. & Witte, C. (2017). Prairie strips improve biodiversity and the delivery of multiple ecosystem services from corn–soybean croplands. *Proceedings of the National Academy of Sciences, 114*(42), 11247-11252.

Shrubsole, D., Brooks, G., Halliday, R., Haque, E., Kumar, A., Lacrois, J., Raisd, H., Rousselle, J., and Simonovic, S. P. (2003) An Assessment of Flood Risk Management in Canada. *Institute for Catastrophic Loss*

Slater, L. J., Singer, M. B., & Kirchner, J. W. (2015) Hydrologic versus geomorphic drivers of trends in flood hazard. *Geophysical Research Letters*, *42*(2), 370–376. https://doi.org/10.1002/2014GL062482

Sommerville, M. & Magnan, A. (2015). 'Pinstripes on the prairies': examining the financialization of farming systems in the Canadian prairie provinces. *Journal of Peasant Studies, 42* (1), 1-26.

Statistics Canada, 1981 Census of Population, Statistics Canada Catalogue no. 97-570-X1981004.

Statistics Canada. (2022). Census Profile. 2021 Census of Population. Statistics Canada Catalogue no. 98-316-X2021001. Ottawa. Released October 26, 2022.

https://www12.statcan.gc.ca/census-recensement/2021/dp-pd/prof/index.cfm?Lang=E (accessed November 1, 2022).

CHAPTER FOUR: CONCLUSIONS

4.1. Summary of Research Findings

Rivers are a landform upon which numerous human settlements have been established. As such, extreme floods pose a risk to infrastructure, agriculture, wildlife, and human life. The scope of human observation of rivers is temporally limited, therefore understanding how extreme floods are recorded in the sedimentary record may extend the record of flooding to improve predictions of future floods and mitigate their hazards.

Point bars are prominent sedimentological features of meandering rivers that are connected to the morphology, sedimentology, and hydrology of meandering rivers. Understanding the morphological change and sedimentary products of extreme floods is essential to refining point bar models. Furthermore, understanding the sedimentary products and causes of extreme floods has implications for improving the prediction of impact and likelihood of future extreme floods events. The objective of this research was to understand the morphology, sedimentology, and hydrology of extreme floods by integrating fieldwork, remote sensing, and statistical modelling. The Assiniboine River in Spruce Woods Provincial Park, Manitoba, was an ideal location for this analysis because of the recent extreme flood events that have significantly altered the geomorphology of the region over the past decade. The breadth of satellite imagery and flow gauge data were critical for this research.

Chapter 2 investigated the geomorphic change and sedimentary deposits of extreme floods using a combination of field work and remote sensing. A field survey was conducted to excavate a series of trenches to observe the internal sedimentology of two point bars and to collect sediment samples. Satellite imagery from Google Earth, Planet Labs, and Esri were used to determine the extent of geomorphic change occurring during floods. LiDAR from fall 2014 and SfM-UAV in summer 2020 were used to construct a DEM and DSM to derive cross-

sectional profiles of the point bar from which we separated extreme flood deposits from annual deposits. This chapter identified five distinct facies present in the two point bars and three vertical grain-size trends, including the typical fining-upwards trend of point bars. The unique coarsening-upward trend was attributed to the change in flow dynamics during extreme floods. However, not all sediment deposited by extreme floods displayed this deviation from the typical point-bar model. The results indicated that 80% of geomorphic change over the past decade had occurred during three extreme floods. The two meander bends migrated mainly by expansion and rotation during extreme floods, although the WRPB did translate downstream during the 2011 flood. The increased rate of migration on the WRPB and FTPB are the result of floodplain heterogeneity and extreme floods that alter bend curvature and increase sediment load. There is some evidence that these sedimentary deposits do vary from the classic point bar facies, displaying a coarsening-upward trend associated with the spread of bar head morphodynamics downstream during extreme floods, but that trend was not always present. The greatest difference between annual flows and extreme floods in the study area was the rate at which migration occurred and the volume of sediment deposited. Studying multiple extreme floods offered insight into how extreme flood deposits can vary from flood to flood and meander bend to meander bend.

Chapter 3 focused on the statistical analysis of the relative contribution of flow frequency and channel capacity to changes in flood hazard on the Assiniboine River using flow gauge data and field measurements from the Holland Gauging Station (Station 05MH005). The flow frequency was analyzed using discharge measurements dating back to 1967 to measure the number of days the river was at or exceeded moderate flood stage. This indicated whether the frequency of moderate flood stage had increased over time. The field measurements used for

stage-discharge data were used to predict what discharge, velocity, and cross-sectional area would be at flood stage. These predicted values were used to determine whether, if flow frequency was held constant, the capacity of the channel had changed over time and extent to which is altered flow frequency. This chapter found that an increase in flow frequency is the greatest cause of increased flood hazard in the region, but that channel capacity has a statistically significant but relatively minor role in decreasing flow frequency. Analysis of the velocity and cross-sectional area components of channel capacity did not have a significant measurable change but due to the local topography it was concluded that area is the dominant control of channel capacity in this region. Understanding the drivers of flooding on the Assiniboine River may aid in improved flood mitigation strategies. Although flow frequency is the greatest driver flood hazard frequency, it is altered by changes in hydroclimatic factors that are difficult to control and predict. Whereas addressing changes to the channel capacity is an immediate solution. Initial results presented in this dissertation suggest the channel is aggrading, increasing the risk of avulsion in the region. Therefore, increasing the cross-sectional area of the channel will lower flood hazard and reduce risks of avulsion.

The results of this dissertation serve to improve our overall understanding of the effect of extreme floods on meandering rivers in semi-confined valleys. It additionally increases our overall understanding of the drivers of flooding on the Assiniboine River. Understanding how extreme deposits are recorded in the sedimentary record may allow for improved recurrence interval analysis on the Assiniboine River, refining flood mitigation strategies.

4.2. Future Work

This research investigated the sedimentology and morphology of two point bars on the Assiniboine River in Spruce Woods Provincial Park and determined the drivers of flood hazard from one gauging station on the river. While the results of each study contribute to our understanding of extreme floods on meandering rivers and flooding on the Assiniboine River, there is still further work that can address why extreme flood deposits vary from flood to flood and meander bend to meander bend. This research will aid in predicting how future floods may impact the region surrounding the river, the extent of changes in channel capacity on the Assiniboine River, and the future risk of avulsion.

The natural progression of the sedimentological and morphological investigation is to further study the two other point bars in the area, the ones that have not migrated significantly over the past decade. This will test the hypothesis that the geomorphology in this region is controlled by antecedent morphology and heterogeneity of the floodplain. Investigating the sedimentary deposits of these two point bars will also provide a frame of reference for the expected deposits when geomorphic change is restricted, allowing for the comparison with point bars that are rapidly migrating. Continued observation of the region will also provide further insight into the behaviour of the meander bends as this study covers a timespan of ten years. Future digital surface models (DSMs) made using the increasingly common RPAS-SfM method can be compared to that created in this study to understand the extent of vertical and lateral geomorphic change on the point bar. Furthermore, subsequent bathymetric surveys in the study reach would progress both investigations conducted in this dissertation. As the point bar migrates laterally, the distribution of channel deposits and their preservation can be extracted from the previous channel position and profile. Additionally, these bathymetric surveys will aid in

understanding how the cross-sectional area of the channel is changing over time, improving the accuracy of analysis in Chapter 3 of the contribution of channel change to flood hazard.

Using the results of Chapter 2 and integrating them with Chapter 3 refines our understanding of the drivers of extreme floods. A major limitation in flood prediction is that discharge measurements are typically limited to human timescales of record keeping. Using our understanding of the deposits of extreme floods in analyzing the sedimentary record of the Assiniboine River may allow for the identification of extreme floods in the region that occurred prior to human observation, increasing the time period used to measure flood frequency. For example, extreme floods may be identified by coarsening-upward sequences similar to those found in the WRPB deposits. In fact, using older data would also improve the accuracy of measuring the channel capacity change. In this study, the field measurements recording changes in velocity and cross-sectional area only spanned a 25-year period compared to the 53 years of flow gauge data.

Chapter 3 applied an established method from Slater et al., (2015) of determining the change in flow frequency, the change in channel capacity, and their relative contributions to flood hazard. It also highlighted the limitations of testing for a monotonic trend when the drivers of these trends (i.e., flow frequency) can have significant decadal variation (i.e., climate). Future work should consider the decadal variation that has been reported in the region (e.g., McCullough et al., 2012; Schindler et al., 2012). Another limitation identified was that flow frequency only tested for duration of flooding (in days per year) and did not measure the magnitude of flooding, which has a significant impact on the flood hazard. Future research may consider quantifying the area under the curve that exceeds moderate flood stage discharge in order to account for the magnitude of flooding in addition to the duration.

Integrating the two investigations further, the 2014 LiDAR data that was utilized for a DEM of the surface of the point bars may also be used to target gauging stations that may benefit from the analysis conducted in Chapter 3. Considering the Assiniboine River's history of avulsion, and the connection between avulsion and channel aggradation, quantifying the change in cross-sectional area of the channel in regions of the river that have become elevated above the floodplain may aid in predicting areas at risk of avulsion. Ultimately, the future work that would be beneficial in understanding extreme floods on the Assiniboine River highlight the importance of multidisciplinary investigations of meandering rivers.

4.3. References

McCullough, G. K., Page, S. J., Hesslein, R. H., Stainton, M. P., Kling, H. J., Salki, A. G., & Barber, D. G. (2012). Hydrological forcing of a recent trophic surge in Lake Winnipeg. *Journal of Great Lakes Research*, *38*, 95-105.

Schindler, D. W., Hecky, R. E., & McCullough, G. K. (2012). The rapid eutrophication of Lake Winnipeg: Greening under global change. *Journal of Great Lakes Research*, *38*, 6-13.

Slater, L. J., Singer, M. B., & Kirchner, J. W. (2015) Hydrologic versus geomorphic drivers of trends in flood hazard. *Geophysical Research Letters*, *42*(2), 370–376. https://doi.org/10.1002/2014GL062482

APPENDIX

Data and code used in Chapter 3 are digital files available upon request.